PCCP

Cite this: *Phys. Chem. Chem. Phys.*, 2011, **13**, 12368–12394

www.rsc.org/pccp

PERSPECTIVE

Recent advances and perspectives in four-component Dirac–Kohn–Sham calculations

Leonardo Belpassi,*[a] Loriano Storchi,[a] Harry M. Quiney[b] and Francesco Tarantelli*[a]

Received 1st March 2011, Accepted 13th May 2011
DOI: 10.1039/c1cp20569b

We review recent theoretical and computational advances in the full relativistic four-component Dirac–Kohn–Sham (DKS) approach and its application to the calculation of the electronic structure of chemical systems containing many heavy atoms. We describe our implementation of an all-electron DKS approach based on the use of G-spinor basis sets, Hermite Gaussian functions, state-of-the-art density-fitting techniques and memory distributed parallelism. This approach has enormously extended the applicability of the DKS method, including for example large clusters of heavy atoms, and opens the way for future key developments. We examine the current limitations and future possible applications of the DKS approach, including the implementation of four-current density functionals and real-time propagation schemes. This would make possible to describe molecules in strong fields, accurately accounting for relativistic kinematic effects and spin–orbit coupling.

1 Introduction

It was Pyykkö and Desclaux,[1] who showed, in the mid-seventies, that relativistic effects, by propagating into the valence region, become very important for chemical bonding. It is now universally recognized that relativistic effects play a crucial role in chemistry, especially when heavy elements are involved. This, and the growing importance of relativistic quantum chemistry, is well documented by a number of dedicated textbooks and review volumes that have been published in the last decade.[2–9]

As hinted to above, if the proper inclusion of relativistic effects in quantum chemical simulations may be important for high-accuracy predictions of spectroscopic observables also for light molecules,[10,11] it is certainly essential for the modelling of molecular systems containing heavy elements. In fact, in this case, there is no alternative to an accurate relativistic treatment if one is to achieve a quantitative description of the electronic structure and properties.

The full relativistic four-component formalism, introduced in 1935 by Bertha Swirles,[12] who put forward for the first time a multielectron Hamiltonian starting from the Dirac equation, has the great advantage of maximal rigour and it affords a physical clarity that is absent in the two-component reductions of the Dirac operator, especially with regard to the problems involved in the change of representation and the gauge dependencies of the electromagnetic interaction. The rigorous relativistic theory offers the natural framework to describe the interaction of particles with electromagnetic fields, as they are both relativistic entities.

Electron correlation is of course as crucial as relativity in determining the electronic structure and electric properties of molecules. These effects are in general not additive and should be treated on the same footing. Due to the large number of electrons that have to be correlated in systems containing heavy atoms, explicit wavefunction-based electron correlation methods rapidly exceed practicability limits, because of their adverse scaling behavior. Indeed, linear scaling techniques may not be particularly useful due to the compactness of molecular systems. A far more practicable approach is offered by Density Functional Theory (DFT) where all the exchange–correlation effects are expressed implicitly by a functional of the electron density. Thus, the problem of describing electron correlation is, in principle, translated into that of devising suitable exchange–correlation functionals, and a huge amount of research efforts is devoted to this today.[13]

As we hinted to above, DFT becomes all the more attractive in the relativistic quantum chemistry domain. A fully relativistic description of atoms, molecules and solids necessarily must be based on quantum electrodynamics (QED). Although relativistic quantum field theories like QED do not provide a Schrödinger-like wave equation for the relativistic many-body problem, there nevertheless exists a well-defined procedure for the derivation of the Hamiltonian and other observables of a stationary system.[14] Utilizing a QED-based Hamiltonian in terms of the four-current,

[a] *Dipartimento di Chimica and CNR-ISTM, Università di Perugia, 06123 Perugia, Italy. E-mail: belp@thch.unipg.it, franc@thch.unipg.it*
[b] *ARC Centre of Excellence for Coherent X-ray Science, School of Physics, The University of Melbourne, Victoria 3010, Australia*

it can be shown that the ground state energy is a unique functional of the ground state four-current $j^{\mu} = (c\rho, \boldsymbol{j})$. Such generalization of the Hohenberg–Kohn theorem to the relativistic domain[15–17] and its extension to the Kohn–Sham framework were put forward more than 30 years ago.[16,18] Engel, Dreizler and collaborators[19,20] have further shown that a rigorous existence proof of a current-density functional within QED can properly be based on renormalized ground state energies and four-currents, taking into account the counter-terms that keep these quantities finite.

The relativistic extension of the Kohn–Sham approach expresses the elementary variables (four-current density) in terms of a set of auxiliary four-component spinors. This representation would permit, through the renormalization procedures of QED, the description of all vacuum corrections to the ground state four-current and energy. However, these corrections are usually irrelevant in practice and accounting for them explicitly would represent a formidable task. While the relativistic variant of the Hohenberg–Kohn theorem guarantees the formal existence of a current-density functional description of relativistic systems, it does not give any hint how to construct such a functional. Because density-current functionals are not yet available, the actual implementations of the Dirac–Kohn–Sham (DKS) scheme usually (pragmatically) resort to the use of non-relativistic functionals.

Many effective numerical implementations of the DKS theory have been presented in the last decade, including the Beijing Density Functional program (BDF) of Liu and coworkers,[21] the program of Fricke and coworkers,[22] the DKS module in the DIRAC program,[23] the DKS module in ReSpect[24] and the REL4D module in Utchem.[25] All these will be reviewed in Section 3. Our own implementation is part of the relativistic code BERTHA.[26–30] Recent theoretical developments have extended the applicability of the DKS methodology to several fields. These include the analysis of the chemical bond in molecules containing heavy and super-heavy atoms,[31] studies of parity violation in chiral molecules,[32–34] the calculation of the electric field gradient (EFG) at the nuclei[35] and other properties. Notable are the implementations of linear,[36,37] quadratic,[38] and cubic[39] response theory schemes, cast in the language of second quantization and based on the quasienergy formalism (Floquet theory).[40] The time-dependent linear response formalism within the four-component DKS theory has been developed for calculating excitation energies, using either a collinear or a non-collinear scheme, for systems containing heavy elements.[41–43] Recently, impressive theoretical achievements have been documented in the prediction of NMR parameters within the framework of DKS theory,[24] with the inclusion of both the magnetic balance and gauge independent atomic orbitals.[44–46] With these prescriptions it has been found that magnetic parameters like shielding tensors are not only independent of the choice of gauge origin but also converge rapidly to the basis set limit.[46]

The major drawback of the full four-component approach is its computational cost, which is intrinsically greater than that of corresponding non-relativistic methods. This originates mainly from the four-component structure of the Dirac equation, the complex matrix representation that usually arises as a consequence, and the increased work involved in the evaluation of the electron density from the auxiliary spinor amplitudes. However, it must be stressed that the increased computational burden arises only as a prefactor in the scaling behaviour: the relativistic four-component formulation does not introduce any new unfavorable scaling with respect to the number of particles or the number of basis functions.

Computationally less demanding methods based on reduced Hamiltonians obtained both at the operator and matrix level have been proposed (see, *e.g.*, ref. 47 and references therein) and one must note that most of the chemistry in the field has so far been produced using these. Maybe the most popular two-component Hamiltonians are the Douglas–Kroll–Hess[48,49] (DKH) and the zeroth-order regular approximation (ZORA)[50–52] Hamiltonian. Both of them have found a wide range of applications in DFT with particularly efficient implementations (see for instance ref. 53 and 54).

As recently reviewed by Liu,[55] techniques to reduce the computational cost of the four-component approach fall into two broad categories, both essentially trying to decouple the solutions of positive and negative energy. In one of them, the aesthetically simple four-component structure is retained but the degrees of freedom associated with the negative energy states are kept frozen.[56,57] In the other, these degrees of freedom are removed by decoupling the large and small components of the Dirac spinors. In the framework of the first paradigm, two- and four-component methods can be made fully equivalent, but then the two-component methods do not offer particular advantages in terms of computational efficiency. The real gain in efficiency can only be achieved by further invoking a model approximation for the small component.[55,56] The second approach can be made self-consistently exact within a given basis set. For recent reviews see ref. 55 and 58.

Aside from theoretical issues concerning the various approximation models, one must recognize that the search for efficient computational strategies to implement the four-component theory is still in its infancy when compared with the decades of computational advances in non-relativistic or quasi-relativistic approaches. Therefore, based on the observation of the not particularly adverse scaling behavior made above, there is ample room for a third, simpler and more direct approach to reduce the cost of four-component relativistic calculations. This is not based on trying to decouple positive and negative energy states but on the attempt to compute more efficiently all the quantities required in a four-component calculation. This entails specific computational developments and the design of new efficient algorithms, which at times may be facilitated by the knowledge accumulated in the non-relativistic context. Significant progress has in fact been made in recent years, through integral screening techniques,[59] pseudospectral methods,[60] and other approaches.[21,61,62] Our specific implementation of the four-component DKS theory is based on the electron-density fitting approach that is already widely used in the non-relativistic context. Numerical density fitting approaches based on an atomic multipolar expansion[21,63] and on a least-squares fit[22] have in fact been employed in the four-component relativistic domain. Recently we have implemented the variational Coulomb fitting approach in our DKS method,[64] with further enhancements resulting from the use of the Poisson equation in the evaluation of the integrals,[65–67] and also from the extension of the density fitting approach to the computation

of the exchange–correlation term.[68] The above algorithmic advances have represented a leap forward of several orders of magnitude in the performance of the four-component DKS approach and have suddenly shifted the computational bottleneck of the method towards the conventional matrix operations (DKS matrix diagonalization, basis transformations, *etc.*) and, especially, to the associated memory demand arising in large-system/large-basis calculations. One powerful approach to tackle these problems and push significantly further forward the applicability limit of all-electron four-component DKS is parallel computation with memory distribution.[69]

This perspective article reviews some of these important computational achievements, and how these can serve as a solid basis for further developments of the full four-component DKS approach. We begin by presenting a brief introduction to relativistic density functional theory and an overview of the available four-component Dirac–Kohn–Sham implementations. We give some details of our effective implementation of the DKS method based on the relativistic code BERTHA,[26–28,30] featuring the use of a G-spinor basis set, density fitting techniques, and memory distributed parallelism. The discussion of a benchmark all-electron application on a large system containing heavy atoms will document the potentiality of the method. We finally outline the areas of further progress that are in our view most important, which concern the development of new four-current density functionals and real-time propagation approaches. These will be key tools for the accurate simulation of molecules in strong fields and of interactions in materials science.

2 Basic theory

The DKS equation with only the longitudinal electrostatic interactions reads

$$\{c\boldsymbol{\alpha}\cdot\boldsymbol{p} + \boldsymbol{\beta}c^2 + v^{(\mathrm{l})}(\boldsymbol{r})\}\boldsymbol{\Psi}_i(\boldsymbol{r}) = \varepsilon_i\boldsymbol{\Psi}_i(\boldsymbol{r}). \tag{1}$$

Here and in the following, except as otherwise noted, atomic units are used. c is the speed of light in vacuum, $\boldsymbol{p}$ is the electron momentum,

$$\boldsymbol{\alpha} = \begin{pmatrix} 0 & \boldsymbol{\sigma} \\ \boldsymbol{\sigma} & 0 \end{pmatrix} \text{ and } \boldsymbol{\beta} = \begin{pmatrix} \boldsymbol{I} & 0 \\ 0 & -\boldsymbol{I} \end{pmatrix} \tag{2}$$

where $\boldsymbol{\sigma} = (\sigma_x,\sigma_y,\sigma_z)$, σ_q is a 2×2 Pauli spin matrix and $\boldsymbol{I}$ is a 2×2 identity matrix. The diagonal potential operator $v^{(\mathrm{l})}(\boldsymbol{r})$ is given by the sum of three terms:

$$v^{(\mathrm{l})}(\boldsymbol{r}) = v_N(\boldsymbol{r}) + v_{\mathrm{H}}^{(\mathrm{l})}[\rho(\boldsymbol{r})] + v_{\mathrm{xc}}^{(\mathrm{l})}[\rho(\boldsymbol{r})] \tag{3}$$

with

$$v_N(\boldsymbol{r}) = \sum_{\mathrm{A}} \int \frac{\rho_{\mathrm{A}}(\boldsymbol{r}')}{|\boldsymbol{r}-\boldsymbol{r}'|}\mathrm{d}\boldsymbol{r}' \tag{4}$$

$$v_{\mathrm{H}}^{(\mathrm{l})}[\rho(\boldsymbol{r})] = \int \frac{\rho(\boldsymbol{r}')}{|\boldsymbol{r}-\boldsymbol{r}'|}\mathrm{d}\boldsymbol{r}' \tag{5}$$

$$v_{\mathrm{xc}}^{(\mathrm{l})}[\rho(\boldsymbol{r})] = \frac{\delta E_{\mathrm{xc}}^{(\mathrm{l})}[\rho(\boldsymbol{r})]}{\delta\rho(\boldsymbol{r})} \tag{6}$$

The potential $v_N[(\boldsymbol{r})]$ represents the scalar external potential due to the fixed nuclei labelled by A, in general described by a finite charge density $\rho_{\mathrm{A}}(\boldsymbol{r})$ and $v_{\mathrm{H}}^{(\mathrm{l})}[\rho(\boldsymbol{r})]$ represents the electronic Coulomb potential due to the electron density $\rho(\boldsymbol{r})$. The Breit interaction contributes to the transverse part of the Hartree interaction ($E_{\mathrm{H}}^{(\mathrm{t})}$) and is not considered here. Note that for the large class of time-reversal invariant systems (that is, closed-shell molecules) $\boldsymbol{j}$ vanishes, so that $E_{\mathrm{H}}^{(\mathrm{t})}$ does not contribute anyway. The term denoted $v_{\mathrm{xc}}^{(\mathrm{l})}[\rho(\boldsymbol{r})]$ is the relativistic longitudinal exchange–correlation potential associated to the longitudinal exchange–correlation energy $E_{\mathrm{xc}}^{(\mathrm{l})}[\rho(\boldsymbol{r})]$. Its exact form is, like that of the corresponding non-relativistic quantity, unknown and has to be approximated. The common non-relativistic density functionals may be used as a first reasonable approximation to which relativistic corrections may be added.[70]

The total energy of the electronic system is given by

$$E_{\mathrm{tot}} = \sum_i \varepsilon_i - E_{\mathrm{H}}^{(\mathrm{l})}[\rho(\boldsymbol{r})] + E_{\mathrm{xc}}^{(\mathrm{l})}[\rho(\boldsymbol{r})] \quad - \int v_{\mathrm{xc}}^{(\mathrm{l})}[\rho(\boldsymbol{r})]\rho(\boldsymbol{r})\mathrm{d}\boldsymbol{r} \tag{7}$$

where the sum extends only over the occupied positive-energy bound states (electronic states). $E_{\mathrm{H}}^{(\mathrm{l})}[\rho(\boldsymbol{r})]$ is just the usual electron Coulomb energy defined as

$$E_{\mathrm{H}}^{(\mathrm{l})}[\rho(\boldsymbol{r})] = \tfrac{1}{2}\int v_{\mathrm{H}}^{(\mathrm{l})}[\rho(\boldsymbol{r})]\rho(\boldsymbol{r})\mathrm{d}\boldsymbol{r}. \tag{8}$$

A four-spinor solution of eqn (1) is of the form

$$\boldsymbol{\Psi}_i(\boldsymbol{r}) = \begin{bmatrix} \psi_i^{(1)}(\boldsymbol{r}) \\ \psi_i^{(2)}(\boldsymbol{r}) \\ \psi_i^{(3)}(\boldsymbol{r}) \\ \psi_i^{(4)}(\boldsymbol{r}) \end{bmatrix}, \tag{9}$$

where the first two components define the so-called "large" (L) component and the last two the "small" (S) component. The total relativistic charge-density is readily evaluated as the scalar product of the four-component spinors according to

$$\rho(\boldsymbol{r}) = \sum_i \boldsymbol{\Psi}_i^{\dagger}(\boldsymbol{r})\cdot\boldsymbol{\Psi}_i(\boldsymbol{r}) = \sum_i \rho_i(\boldsymbol{r}) \tag{10}$$

where the sum again extends only over the occupied positive-energy states. The scalar product of a DKS spinor $\boldsymbol{\Psi}_i(\boldsymbol{r})$ with itself is defined to be

$$\rho_i(\boldsymbol{r}) = \boldsymbol{\Psi}_i^{\dagger}(\boldsymbol{r})\cdot\boldsymbol{\Psi}_i(\boldsymbol{r}) = \sum_{\mu=1}^{4} \psi_i^{(\mu)*}(\boldsymbol{r})\psi_i^{(\mu)}(\boldsymbol{r}) \tag{11}$$

Also the total current density, $\boldsymbol{j} = (j_x,j_y,j_z)$, can be expressed *via* the single-particle Dirac spinors as

$$\boldsymbol{j} = c\sum_i \boldsymbol{\Psi}_i^{\dagger}(\boldsymbol{r})\alpha\Psi_i(\boldsymbol{r}) \tag{12}$$

where $c\boldsymbol{\alpha} = (c\boldsymbol{\alpha}_x,c\boldsymbol{\alpha}_y,c\boldsymbol{\alpha}_z)$ denotes, as before, the 4×4 matrix representation of the relativistic electron current operator. Also in this case the sum extends only over the occupied

positive-energy states. The principal computational task in DKS is the determination of the spinors, which are the single-particle solutions of the Dirac equation constructed for some effective potential.

3 Current implementations and typical applications

In this section we want to briefly review some of the current documented implementations of the DKS theory. Historically, the first program for the construction of relativistic self-consistent field approximations for molecular applications using a spinor structure was probably that of Rosén and Ellis in the seventies.[71,72] The program used numerical basis sets of four-component wavefunctions obtained from atom-like Dirac–Slater wavefunctions and used Slater's exchange functional. The approach implemented a discrete variational method and was applied to the study of small molecules like for instance XeF_2.

In the same years Yang and co-workers[73,74] and Cartling and Whitmore[75,76] introduced a scattered-wave formalism based on the four-component Dirac equation for a "muffin-tin" potential. These self-consistent Dirac–Slater multiple scattering calculations produced useful chemical insight in a number of applications (see for instance ref. 74 and 77–79).

3.1 The program of Fricke *et al.*

Ellis' program was subsequently substantially improved by the group of Fricke.[80,81] This implementation was based on the variationally consistent Coulomb density fitting procedure with all required integrals evaluated numerically.[82] Applications were reported for the binding energies, bond lengths, vibrational frequencies and potential energy curves of ground-state diatomic molecules containing heavy atoms.[83] The gradient of the exchange–correlation functionals and their relativistic correction (RLDA, RGGA) were introduced and investigated in a systematic study of molecules including Cu_2, Ag_2, and Au_2.[84] The results indicated that the relativistic corrections to absolute total energies are significant but their contributions largely cancel out when computing dissociation energies.[22,84] The potential energy surface of diatomic molecules has been also investigated[22] but the accuracy of the results was questioned (see ref. 85 and 86). Analytical gradients were implemented[87] and the code was used, for example, in a study of CO adsorption on heavy metal clusters implementing the frozen core approximation.[88] More recently, the code has been extended with an effective implementation of both the non-collinear and collinear schemes of relativistic density functional theory.[89–92] The method implemented is purely numeric and the DKS equation was solved using numerical atomic orbitals as basis functions. The computation of the Hartree potential is based on an approximated multipole multicenter expansion of the molecular electron density. In particular, it takes advantage of the use of a model density which is expanded in multicenter multipolar fitting basis functions.[90] In the current implementation, the fitting functions are radial subshell densities multiplied by spherical harmonics. The code has been applied extensively in recent years to the study of super-heavy elements and their absorption on metal surfaces.[93–97]

3.2 The BDF program

Ellis' program also served as the starting point for the development of the Beijing Density Functional program (BDF)[21,63] carried out by the group of Liu. The program is based on a numerical integration scheme for the evaluation of the multicenter two-electron integrals. In order to evaluate the matrix elements of the Hartree potential first, the density is decomposed into disjoint atomic contribution based on the partition functions of Becke, from which a multipolar expansion is made. While the Hartree potential for each term of the multipolar expansion at each grid point can be evaluated accurately using one-dimensional numerical integration, the multipolar expansion of the electron density itself has to be truncated, and this truncation is the numerical parameter controlling the accuracy. Three different polarization schemes, *viz*. Kramers-unrestricted, collinear, and noncollinear, have been implemented in the code. Systematic comparisons have been presented to assess their performance.[98] The program has been recently extended to use full molecular symmetry, including both double point groups and time-reversal.[99] In the context of the development of this program, the first time-dependent four-component relativistic DFT implementation, within the linear response regime, has been presented for the calculation of excitation energies including spin–orbit coupling.[41] This pivotal implementation has further been extended by using a non-collinear form for the exchange–correlation kernel that allows excited states involving "spin-flipped" configurations.[42] An effective implementation has been developed for the DKS calculation of the magnetic shielding tensor for molecules. These calculations are not only independent of the choice of gauge origin but also converge rapidly to the basis set limit. This remarkable achievement has been obtained using magnetically balanced atomic orbitals having each its own local gauge origin placed in its center. The implementation of this formalism is now available in BDF.[46]

3.3 The Utchem program

The DKS module that is implemented in REL4D,[25,100,101] part of Utchem code,[102] due to Yanai *et al*., is based on the expansion of the four-component molecular spinors in generally contracted, spherical harmonic, two-component, Gaussian-type spinors. The four-index repulsion integrals are computed analytically, using an efficient scheme to handle contracted Gaussian functions.[103,104] The algorithm has been improved[100] combining the ACE method[104] and the transfer relations derived by Head-Gordon and Pople.[105] The two-electron repulsion integrals are then multiplied by the density matrix in order to generate the Coulomb matrix. The numerical grid-quadrature routine for the exchange–correlation potentials is based on the non-relativistic DFT code developed by Tsuneda and Hirao.[106] The module includes the implementation of the pseudospectral (PS) approach of Friesner.[107] This approach allowed for an efficient inclusion of exchange–correlation functionals exhibiting the exact exchange potential. This approach appears promising, but its effective application is so far limited to a study of the hexacarbonyl complexes of tungsten and seaborgium.[60] Recently, this implementation has been extended to use double-group symmetry.[108] The use of double-group symmetry entails significant computational efficiencies. Some benchmark results have been reported for molecules like UF_6.[108]

3.4 The DIRAC program

Among the current four-component relativistic programs, the DIRAC package[109] is perhaps the most complete and versatile. Its DKS module, due to Saue and Helgaker,[23] derives from its Dirac–Fock program, with all electron repulsion integrals evaluated analytically. The implementation is based on a scheme that makes efficient use of symmetries, like time-reversal of D_{2h} and its subgroups. Time-reversal symmetry is handled by use of the quaternion algebra.[110] Each component of a four-spinor results expanded in a Cartesian Gaussian-type scalar atomic basis set. This allows the use of the same analytical and numerical integral evaluation routines that are used in the non-relativistic DALTON code.[111] Besides the use of integral screening,[59] the module implements the simple Coulomb correction proposed by Visscher[62] that models very well the contribution of (*SS*–*SS*) integrals, thus eliminating their calculations and thereby achieving substantial computational savings. The code can use both contracted and uncontracted basis sets. The exchange–correlation matrix elements are computed by the numerical integration scheme based on the Becke partitioning of the molecular volume into atomic regions,[112] where quadrature is performed in spherical coordinates. The DKS matrix construction is effectively parallelized in data-distribution mode. The code implements several non-relativistic exchange–correlation functionals including several generalized gradient approximation (GGA) ones, hybrid-functionals, and the gradient regulated asymptotic correction scheme[113] (GRAC) and the statistical averaging of (model) orbital potentials (SAOP) as defined in ref. 114. The code has been used in a wide range of applications such as, for instance, analysis of chemical bonds,[115] the study of parity violation[32,34,116,117] and properties like the EFG.[35] The formalism used in DIRAC is based on an exponential parametrization of the non-interacting Kohn–Sham reference determinant and is well-suited for the applications of linear and non-linear response theory under weak perturbations. The recent developments in this area are impressive and both linear[36,37,118] and quadratic[38] response DFT based on the four-component Dirac–Coulomb Hamiltonian are now available. The theory is cast in the language of second quantization and is based on the quasienergy formalism[40] replacing the initial state dependence of the Runge–Gross theorem[119] by periodic boundary conditions. Furthermore, an implementation of cubic response theory has recently been presented[39] which permits, for the first time, the analytic calculations of the second hyperpolarizability in a relativistic framework. Benchmark calculations for the hydrogen halides have shown that relativistic effects can indeed be substantial for frequency-dependent second hyperpolarizabilities. Bast *et al.*[43] report an implementation of adiabatic time-dependent density functional theory based on the four-component relativistic Dirac–Coulomb Hamiltonian and a closed-shell reference. The implementation includes noncollinear spin magnetization and full derivatives of functionals,[120] including hybrid GGA functionals. The performance of various functionals for calculating $ns^2ns^2 \rightarrow ns^1np^1$ excitation energies in Zn, Cd, and Hg, as well as the vertical excitation energies of UO_2^{2+} molecules, has been also investigated. The results show that GGA functionals, such as, for example, BLYP, perform remarkably well for group 12 atoms hcl, whereas hybrid functionals tend to underestimate excitation energies. In the case of uranyl, it appears that long-range corrected functionals show the best performance. The results indicate that the adiabatic local density approximation (ALDA) is a good approximation for some GGA functionals, but not all. Furthermore, it appears that ALDA is an extremely bad approximation for hybrid functionals. Important developments have been achieved in the visualization of molecular properties.[121,122] In this respect, for instance, Bast *et al.*[121] have recently presented a four-component relativistic implementation for calculating the magnetically induced current density within DKS linear response theory using a common gauge origin. This opens up the possibility to investigate magnetically induced current densities of aromatic systems containing heavy elements with both scalar relativistic and spin–orbit effects included.

3.5 The ReSpect program

A new relativistic four-component DFT module has been developed within the code ReSpect[24,44,123] due to a collaboration of Kaupp in University of Würzburg and Malkin at the Slovak Academy of Sciences in Bratislava. It has been applied to the calculations of NMR shielding tensors[24] and indirect nuclear spin–spin coupling constants.[123] It is based on the matrix formulation of the DKS method. Initially, unperturbed equations are solved with the use of a restricted kinetically balanced basis set for the small component. The second-order coupled perturbed DKS method is then based on the use of restricted magnetically balanced basis sets for the small component. Benchmark relativistic calculations have demonstrated the high reliability of such an approach. Very recently, this method has been extended to calculations of electronic *g*-tensors.[44] The authors show that this four-component code not only provides a reference against which other more approximate methods may be benchmarked, but it can also be used effectively in real chemical applications. Calculations carried out on molecules like WO(benzene-1,2-dithiolate)$_2^-$ have exhibited a degree of efficiency comparable to that of existing approximate two-component methods with transformed Hamiltonians (such as the DKH method, the zero-order regular approximation (ZORA)[50–52] or related approaches) with the clear advantage that it has no picture change effects.

Finally, we mention that a number of DKS implementations have been presented for solid state calculations (see for instance ref. 124–129).

4 The DKS implementation in BERTHA

In this section we review the main features of the implementation of the DKS method in the four-component code BERTHA.[2] This DKS code[26] was basically built around a particularly efficient algorithm for electronic repulsion integrals developed by Quiney and Grant more than a decade ago (see ref. 2 and 3), which represents a relativistic generalization of the well-known McMurchie–Davidson algorithm.[130] Up to that time four-component codes had generally only been applied to diatomic or polyatomic molecules with at most one heavy atom. Since then, in a continuous development including the recent introduction of efficient density-fitting techniques and parallelization strategies,

the range of applicability of the code has been extended enormously.

The four-component formulation of relativistic DFT which is implemented in BERTHA uses an uncontracted Gaussian basis set expansion. The basis functions employed are termed G-spinors (see page 544 of ref. 2). These functions are two-component spin–orbit coupled objects derived from the SGTF (Spherical Gaussian Type Function) basis.[131] The G-spinors do not suffer from the variational problems of kinetic balance (see ref. 132 and references therein) and, regarding the evaluation of multicentre integrals, retain the advantages which have made Gaussian-type functions the most widely-used expansion set in non-relativistic quantum chemistry. G-spinors are designed to have the same transformational properties as central field atomic four-spinors. They are eigenfunctions of the total (spin–orbit) angular momentum operators j^2 and j_z, and of the Johnson–Lippmann fine-structure operator[26] with eigenvalues $\kappa = \pm1, \pm2, \pm3,\ldots$.

A G-spinor consists of two components of the form

$$M_\mu^{(\mathrm{L})}(\boldsymbol{r}) = \frac{f_\mu^{(\mathrm{L})}(r)}{r}\chi_{\kappa,m_j}(\theta,\varphi) \tag{13}$$

$$M_\mu^{(\mathrm{S})}(\boldsymbol{r}) = i\frac{f_\mu^{(\mathrm{S})}(r)}{r}\chi_{-\kappa,m_j}(\theta,\varphi) \tag{14}$$

where the labels L and S denote the large and small components, respectively. In the following, the generic component label L or S will be denoted by T. The $f_\mu^{(\mathrm{T})}(\boldsymbol{r})$ are radial functions and $\chi_{\kappa,m_j}(\theta,\varphi)$ are spin-angular functions[26] constructed from spherical harmonic functions in a two-component space of spin eigenfunctions. The index μ may be thought of as the collection of parameters necessary to completely characterize the functions: $\mu = (\kappa,m_j,\lambda,\boldsymbol{A})$. It comprises the fine-structure quantum number κ, the quantum number associated to the z component of the angular momentum, m_j, the Gaussian exponent λ, and the origin of the local coordinate system $\boldsymbol{r}_\mathrm{A}$. It is often convenient to label the G-spinors using the nominal orbital angular momentum label, l, because this makes the correspondence with non-relativistic theory more immediate. This is very useful from a practical point of view for the construction of relativistic basis sets starting from a conventional non-relativistic definition of the basis functions. The relationship that links l to the atomic relativistic quantum numbers is $l = \kappa/(2j+1) + j$. Conversely, if l is given, this specifies the associated G-spinors that have $j = l \pm \frac{1}{2}$, $\kappa = (l-j)(2j+1)$ and $-j \leq m_j \leq j$. The quantum number j is related to κ by $j = (2|\kappa| - 1)/2$. The functional relationship between large- and small-component basis functions is determined by the kinetic balance prescription, $M_\mu^{(\mathrm{S})}(\boldsymbol{r}) \propto \boldsymbol{\sigma}\cdot\boldsymbol{p}M_\mu^{(\mathrm{L})}(\boldsymbol{r})$. The function $f_\mu^{(\mathrm{L})}(\boldsymbol{r})$ is the radial part of a spherical harmonic Gaussian-type function[131] defined in a coordinate system centred at $\boldsymbol{r}_\mathrm{A}$,

$$f_\mu^{(\mathrm{L})}(r) = N^{(\mathrm{L})}r_\mathrm{A}^{l+1}\exp(-\lambda r_\mathrm{A}^2) \tag{15}$$

with $r_\mathrm{A} = |\boldsymbol{r} - \boldsymbol{r}_\mathrm{A}|$. The restricted, kinetically matched (see ref. 26) radial small component function is then

$$f^{(\mathrm{S})}(r) = N^{(\mathrm{S})}[(\kappa + l + 1) - 2\lambda r_\mathrm{A}^2]r_\mathrm{A}^l\exp(-\lambda r_\mathrm{A}^2) \tag{16}$$

where $N^{(\mathrm{L})}$ and $N^{(\mathrm{S})}$ are normalization factors. The two-component angular functions are defined by

$$\chi_{\kappa,m_j}(\theta,\varphi) = \begin{bmatrix} -\left(\frac{j+1-m_j}{2j+2}\right)^{1/2} Y_{j+1/2}^{m_j-1/2}(\theta,\varphi) \\ \left(\frac{j+1+m_j}{2j+2}\right)^{1/2} Y_{j+1/2}^{m_j+1/2}(\theta,\varphi) \end{bmatrix} \tag{17}$$

and

$$\chi_{\kappa,m_j}(\theta,\varphi) = \begin{bmatrix} \left(\frac{j+m_j}{2j}\right)^{1/2} Y_{j-1/2}^{m_j-1/2}(\theta,\varphi) \\ \left(\frac{j-m_j}{2j}\right)^{1/2} Y_{j-1/2}^{m_j+1/2}(\theta,\varphi) \end{bmatrix} \tag{18}$$

for $\kappa > 0$ and $\kappa < 0$, respectively, where the spherical harmonic functions $Y_l^m(\theta,\phi)$ are as defined by Condon and Shortley.[133]

The choice of the basis set is strictly linked to the model of the nuclei that is adopted. For heavy nuclei, a point model is an unsuitable physical description, particularly if we are interested in effects due to the surrounding electron density. We must thus choose a suitably parameterized model of the nuclear charge density distribution. Studies of the electronic structure have shown that the electron density is sensitive to the mean-square radius of the nuclear charge density and to the magnitude of the potential at the center of mass of the nucleus, not to the details of the nuclear charge distribution. A spherically symmetric Gaussian charge distribution of the form

$$\rho_\mathrm{A}(r) = Z\left(\frac{\lambda_\mathrm{A}}{\pi}\right)^{3/2}\exp(-\lambda_\mathrm{A}r^2) \tag{19}$$

is therefore used, where (r,θ,ϕ) is a spherical polar coordinate system whose origin is at the center of mass of the nucleus and λ_A is a positive constant related to the root-mean-square radius of the nucleus. The exponent λ_A may be determined by fitting the rms radius of the Gaussian function to experimental values obtained from electron scattering experiments. In BERTHA we use the formulae for the nuclear Gaussian exponent, λ_A, suggested by Visscher and Dyall.[134] The use of the G-spinor basis set, coupled with a finite charge distribution model for the nuclei, is particularly advantageous. In particular it guarantees that the boundary conditions for $r \to 0$ imposed by the Dirac equation on the ratio of its large- and small-component solutions are satisfied.[135] In addition, it provides a consistent model, in that the exact radial solutions of the Dirac equation approach a Gaussian form near the nuclei for a finite nuclear charge distribution.

The spinor solution of the DKS equation (eqn (1)) is thus expressed as a linear combination of G-spinor basis functions as

$$\boldsymbol{\Psi}_i(\boldsymbol{r}) = \begin{bmatrix} \sum_{\mu=1}^N c_{\mu i}^{(\mathrm{L})} M_\mu^{(\mathrm{L})}(\boldsymbol{r}) \\ i\sum_{\mu=1}^N c_{\mu i}^{(\mathrm{S})} M_\mu^{(\mathrm{S})}(\boldsymbol{r}) \end{bmatrix}, \tag{20}$$

where, $c_{\mu i}^{(\mathrm{T})}$ are coefficients to be determined and N is the number of basis functions. In the G-spinor representation, the density matrices are

$$D_{\mu\nu}^{(\mathrm{TT}')} = \sum_i c_{\mu i}^{(\mathrm{T})*} c_{\nu i}^{(\mathrm{T}')} \tag{21}$$

where the sum runs over the occupied positive-energy states. The total electron density is then readily obtained as

$$\rho(\boldsymbol{r}) = \sum_{\mathrm{T}} \sum_{\mu,\nu} D_{\mu\nu}^{(\mathrm{TT})} \rho_{\mu\nu}^{(\mathrm{TT})}(\boldsymbol{r}) \tag{22}$$

and the current can be expressed as

$$j_q(\boldsymbol{r}) = \sum_{\mathrm{T}\neq\mathrm{T}'} \sum_{\mu,\nu} D_{\mu\nu}^{(\mathrm{TT}')} j_{q,\mu\nu}^{(\mathrm{TT}')}(\boldsymbol{r}) \tag{23}$$

with $q = x,y,z$. The terms $\rho_{\mu\nu}^{(\mathrm{TT})}(\boldsymbol{r})$ and $j_{q,\mu\nu}^{(\mathrm{TT}')}(\boldsymbol{r})$ are the G-spinor overlap densities and overlap current densities, respectively. These quantities can be expressed as linear combinations of quantities derived from two-component objects, according to the rules:

$$\begin{aligned} \rho_{\mu\nu}^{(\mathrm{TT})}(\boldsymbol{r}) &= M_{\mu}^{(\mathrm{T})\dagger}(\boldsymbol{r}) M_{\nu}^{(\mathrm{T})}(\boldsymbol{r}) \\ &= \sum_{ijk} E_0^{(\mathrm{TT})}[\mu,\nu;i,j,k] H[\alpha_{\mu\nu};i,j,k;\boldsymbol{r}] \end{aligned} \tag{24}$$

$$\begin{aligned} j_{q,\mu\nu}^{(\mathrm{TT}')}(r) &= c M_{\mu}^{(\mathrm{T})\dagger}(\boldsymbol{r}) \boldsymbol{\sigma}_q M_{\nu}^{(\mathrm{T}')}(\boldsymbol{r}) \\ &= \sum_{ijk} E_q^{(\mathrm{TT}')}[\mu,\nu;i,j,k] H[\dot{\alpha}_{\mu\nu};i,j,k;\boldsymbol{r}] \end{aligned} \tag{25}$$

These are finite superpositions, with coefficients E_0 and E_q, of standard Hermite Gaussian-type functions (HGTFs) $H[\alpha_{\mu\nu};i,j,k;\boldsymbol{r}]$, defined by

$$H[\alpha,\boldsymbol{r}_{\mathrm{A}};i,j,k;\boldsymbol{r}] = \frac{\partial^i}{\partial x^i}\frac{\partial^j}{\partial y^j}\frac{\partial^k}{\partial z^k} \mathrm{e}^{-\alpha|\boldsymbol{r}-\boldsymbol{r}_{\mathrm{A}}|^2} \tag{26}$$

The index $\alpha_{\mu\nu}$ concisely identifies both the HGTF origin and exponent which result from application of the Gaussian product theorem on the basis functions labeled by μ and ν (see, *e.g.*, ref. 131). The E_0 and E_q coefficients, which contain the whole spinor structure, are described in ref. 136 and 137 and have been further generalized using effective recurrence relations[138] (see page 779 of ref. 2). The ranges of the summations over i, j and k in eqn (24) and (25) are determined uniquely by the indices that specify the basis functions: it is possible to show that the above expansion of the four-current density is restricted by the conditions $0 \leq i + j + k \leq \ell_\mu + \ell_\nu$ for the large component, and $0 < i + j + k \leq \ell_\mu + \ell_\nu + 2$ for the small component, where ℓ_μ and ℓ_ν are the angular momentum quantum numbers of the two spinors involved. Thus, the total number of terms in the summation is

$$N_\Lambda = \frac{(\Lambda+1)(\Lambda+2)(\Lambda+3)}{6} \tag{27}$$

where $\Lambda = \ell_\mu + \ell_\nu$ for T = L and $\Lambda = \ell_\mu + \ell_\nu + 2$ for T = S. The definition and construction of the E_0 and E_q coefficients enables the efficient analytic evaluation of all multi-centre G-spinor Coulomb integrals, using a relativistic generalization of the McMurchie–Davidson algorithm.[130,131] Other significant advantages of this approach will emerge clearly in the course of the following discussion.

The matrix representation of the DKS operator is given by

$$\boldsymbol{H}_{\mathrm{DKS}} = \begin{bmatrix} \boldsymbol{V}^{(\mathrm{LL})} + mc^2\boldsymbol{S}^{(\mathrm{LL})} & c\boldsymbol{\Pi}^{(\mathrm{LS})} \\ c\boldsymbol{\Pi}^{(\mathrm{SL})} & \boldsymbol{V}^{(\mathrm{SS})} - mc^2\boldsymbol{S}^{(\mathrm{SS})} \end{bmatrix} \tag{28}$$

where

$$\boldsymbol{V}^{(\mathrm{TT})} = \boldsymbol{v}^{(\mathrm{TT})} + \boldsymbol{J}^{(\mathrm{TT})} + \boldsymbol{K}^{(\mathrm{TT})} \tag{29}$$

The associated eigenvalue equation reads

$$\boldsymbol{H}_{\mathrm{DKS}} \begin{bmatrix} \boldsymbol{c}^{(\mathrm{L})} \\ \boldsymbol{c}^{(\mathrm{S})} \end{bmatrix} = E \begin{bmatrix} \boldsymbol{S}^{(\mathrm{LL})} & 0 \\ 0 & \boldsymbol{S}^{(\mathrm{SS})} \end{bmatrix} \begin{bmatrix} \boldsymbol{c}^{(\mathrm{L})} \\ \boldsymbol{c}^{(\mathrm{S})} \end{bmatrix} \tag{30}$$

where $\boldsymbol{c}^{(\mathrm{T})}$ are the spinor expansion vectors of eqn (20). The matrices $\boldsymbol{v}^{(\mathrm{TT})}$, $\boldsymbol{J}^{(\mathrm{TT})}$, $\boldsymbol{K}^{(\mathrm{TT})}$, $\boldsymbol{S}^{(\mathrm{TT})}$, and $\boldsymbol{\Pi}^{(\mathrm{TT}\prime)}$ appearing above are, respectively, the basis representations of the nuclear, Coulomb, and exchange–correlation potentials, the overlap matrix, and the matrix of the kinetic energy operator. Their matrix elements are defined by

$$v_{\mu\nu}^{(\mathrm{TT})} = \int v_N(\boldsymbol{r}) \rho_{\mu\nu}^{(\mathrm{TT})}(\boldsymbol{r}) \mathrm{d}\boldsymbol{r} \tag{31}$$

$$J_{\mu\nu}^{(\mathrm{TT})} = \int v_{\mathrm{H}}^{(\mathrm{l})}[\rho(\boldsymbol{r})] \rho_{\mu\nu}^{(\mathrm{TT})}(\boldsymbol{r}) \mathrm{d}\boldsymbol{r} \tag{32}$$

$$K_{\mu\nu}^{(\mathrm{TT})} = \int v_{\mathrm{xc}}^{(\mathrm{l})}[\rho(\boldsymbol{r})] \rho_{\mu\nu}^{(\mathrm{TT})}(\boldsymbol{r}) \mathrm{d}\boldsymbol{r} \tag{33}$$

$$S_{\mu\nu}^{(\mathrm{TT})} = \int \rho_{\mu\nu}^{(\mathrm{TT})}(\boldsymbol{r}) \mathrm{d}\boldsymbol{r} \tag{34}$$

$$\Pi_{\mu\nu}^{(\mathrm{TT}')} = \int M_{\mu}^{(\mathrm{T})\dagger}(\boldsymbol{r}) (\boldsymbol{\sigma}\cdot\boldsymbol{p}) M_{\nu}^{(\mathrm{T}')}(\boldsymbol{r}) d\boldsymbol{r} \tag{35}$$

The matrix $\boldsymbol{H}_{\mathrm{DKS}}$ depends, through the ρ in $v_{\mathrm{xc}}^{(\mathrm{l})}[\rho(\boldsymbol{r})]$ and $v_{\mathrm{H}}^{(\mathrm{l})}[\rho(\boldsymbol{r})]$, on the canonical spinor-orbitals produced by its diagonalization, so that the solution ($\boldsymbol{c}^{(\mathrm{T})}$) must be obtained recursively to self-consistence.

The most demanding computational task in a DKS calculation using the G-spinor expansion is the evaluation of the Coulomb and exchange–correlation contributions to the DKS matrix, eqn (32) and (33), respectively. For each of these matrices a different strategy is adopted. The multicentre integrals of the exchange–correlation functional $v_{\mathrm{xc}}[\rho(\boldsymbol{r})]$ that define the exchange–correlation matrix are evaluated numerically using the methods described by Becke.[112] To every point in space, $\boldsymbol{r}_i$, in the numerical quadrature grid, is associated a set of weight functions, $\{w_{\mathrm{A}}(\boldsymbol{r}_i)\}$, where A labels the nuclear centre to which the weight function belongs. In this way, any integrand, $F(\boldsymbol{r}_i)$, is apportioned into a corresponding set of contributions, $F_{\mathrm{A}}(\boldsymbol{r}_i) = w_{\mathrm{A}}(\boldsymbol{r}_i)F(\boldsymbol{r}_i)$, one for each nucleus. The quadratures involving the angular variables are evaluated using angular weights, $\{w_i\}$, and abscissae, $\{\theta_i,\varphi_i\}$, using the Lebedev quadrature scheme. The weights and abscissae of the Lebedev integration scheme have been reported by Lebedev and Laikov.[139] Further details may be found in ref. 26.

The Coulomb matrix $\boldsymbol{J}^{(\mathrm{TT})}$, which involves 6-dimensional two-electron repulsion integrals, is computed analytically on the basis of a generalization of the *J*-matrix algorithm developed in non-relativistic quantum chemistry.[140,141] This approach is a key feature of BERTHA and is summarized in the following section.

4.1 The relativistic *J* matrix

In the G-spinor representation the total charge density, using eqn (22) and (24), can readily be obtained as

$$\rho(\boldsymbol{r}) = \sum_{\alpha} \sum_{i,j,k} H[\alpha; i,j,k; \boldsymbol{r}] H_0[\alpha; i,j,k] \tag{36}$$

The coefficients $H_0[\alpha;i,j,k]$, which are the relativistic analogue of the scalar Hermite density matrix proposed by Almlöf,[140,141] are given by

$$H_0[\alpha; i,j,k] = \sum_{\mathrm{T}} \sum_{\mu,\nu\rightarrow\alpha} E_0^{(\mathrm{TT})}[\mu,\nu; i,j,k] D_{\mu\nu}^{(\mathrm{TT})}, \tag{37}$$

where the second sum runs over all basis function pairs resulting, by the Gaussian product theorem, in the same origin and exponent labeled by α. The large-component Hermite set is a subset of the small-component set as a consequence of kinetic balance and the matching of functions. The efficiency of this approach increases with increasing angular momentum (more density is accumulated in the sum over $\{\mu,\nu\}$). Although the form of the coefficients $H_0[\alpha;ijk]$ is the same as in the non-relativistic case, their number is larger because the possible indices $\{ijk\}$ are determined by the small component. For fixed angular momenta, ℓ and ℓ', the number of extra terms is

$$\frac{(\Lambda+4)(\Lambda+5)}{(\Lambda+1)(\Lambda+2)} \tag{38}$$

where $\Lambda = \ell + \ell'$. This corresponds to an increase of about two for two *f* functions.

The *J* matrix elements, eqn (32), in terms of the G-spinor basis set and HGTFs, are given by

$$\begin{aligned} J_{\mu\nu}^{(\mathrm{TT})} &= \sum_{i,j,k} E_0^{(\mathrm{TT})}[\mu,\nu; i,j,k] \\ &\quad \times \int v_{\mathrm{H}}^{(\mathrm{l})}[\rho(\boldsymbol{r})] H[\alpha_{\mu\nu}; i,j,k; \boldsymbol{r}] \mathrm{d}\boldsymbol{r} \\ &= \sum_{i,j,k} E_0^{(\mathrm{TT})}[\mu,\nu; i,j,k] \langle \alpha_{\mu\nu}; ijk | v_{\mathrm{C}} \rangle \end{aligned} \tag{39}$$

where, we have used the symbol

$$\langle \alpha_{\mu\nu}; ijk | v_{\mathrm{C}} \rangle = \sum_{\alpha'} \sum_{i',j',k'} \langle \alpha_{\mu\nu}; ijk \parallel \alpha'; i'j'k' \rangle H_0[\alpha'; i',j',k'] \tag{40}$$

This is a linear combination of the usual Gaussian Coulomb two-electron integrals

$$\begin{aligned} \langle \alpha; ijk \parallel \alpha'; i'j'k' \rangle &= \int H[\alpha; i,j,k; \boldsymbol{r}] \frac{1}{|\boldsymbol{r}-\boldsymbol{r}'|} \\ &\quad H[\alpha'; i',j',k'; \boldsymbol{r}'] \mathrm{d}\boldsymbol{r} \mathrm{d}\boldsymbol{r}' \end{aligned} \tag{41}$$

involving intermediate HGTFs, which are commonly computed also in standard non-relativistic quantum chemistry codes.[131] For α' corresponding to two *f*-functions, this may be estimated to be between 50 and 100 times faster than calculating two-electron G-spinor integrals to obtain the same quantity. The total Coulomb energy, E_J, is then given by

$$E_J = \frac{1}{2} \sum_{\mathrm{T}} \sum_{\mu,\nu} D_{\mu\nu}^{(\mathrm{TT})} J_{\mu\nu}^{(\mathrm{TT})} \tag{42}$$

The *J*-matrix approach of eqn (39), compared with the summation over two-electron integrals used by other four-component density functional codes, turns out to be particularly efficient. Using this expansion, the costly transformation from the integrals over the HGTF basis to the four-index two-electron set of G-spinor integrals is avoided. This permits dramatic simplifications[140] when several atomic basis functions have an identical exponent and especially when the contributing spinors have large angular momentum. It should be underlined that if large angular momentum basis functions are often important for high-accuracy results in general, they become routinely indispensable for calculations on molecular systems containing heavy atoms. The Hermite expansion of the current density is given by

$$j_q(\boldsymbol{r}) = \sum_{\alpha} \sum_{i,j,k} H[\alpha; ijk; \boldsymbol{r}] H_q[\alpha; ijk] \tag{43}$$

The coefficients appearing here are defined as

$$\begin{aligned} H_q[\alpha; ijk] &= \sum_{\mu,\nu\rightarrow\alpha} \{ E_q^{(\mathrm{LS})}[\mu\nu; i,j,k] D_{\mu\nu}^{(\mathrm{LS})} \\ &\quad + E_q^{(\mathrm{SL})}[\mu\nu; i,j,k] D_{\mu\nu}^{(\mathrm{SL})} \} \end{aligned} \tag{44}$$

with $q = x,y,z$.

Once one has constructed these modified densities, other important quantities can be easily derived using the properties of the HGTFs, much as it is done in non-relativistic algorithms. For example, the *x* component of the gradient of the electronic density reads

$$\frac{\partial \rho(\boldsymbol{r})}{\partial x} = -\sum_{\alpha} \sum_{i,j,k} H[\alpha; i+1,j,k; \boldsymbol{r}] H_0[\alpha; i,j,k] \tag{45}$$

without any explicit reference to the G-spinor structure. This clearly shows that all essential required quantities in a relativistic DFT theory can be expressed as a simple linear combination of scalar functions such as Hermite Gaussian functions, with all the spinor structure absorbed in the modified densities, which are real, scalar quantities. Besides computational efficiency this approach is conceptually very simple and direct. This has proved to be a key feature in facilitating the new algorithmic developments and code maintenance we have undertaken in the last few years.

4.2 Coulomb and Poisson density fit

The total relativistic density, exactly like its non-relativistic counterpart, is a real scalar function that can usefully be approximated using an auxiliary atom-centred basis set:

$$\tilde{\rho}(\boldsymbol{r}) = \sum_{t=1}^{N_{\mathrm{aux}}} d_t f_t(\boldsymbol{r}) \tag{46}$$

where N_{aux} is the number of auxiliary basis functions. According to the most widely used approach,[142–147] the coefficients d_t are chosen to minimize the error Δ in the Coulomb energy:

$$\Delta = \int \delta\rho(\boldsymbol{r}) \frac{1}{|\boldsymbol{r}-\boldsymbol{r}'|} \delta\rho(\boldsymbol{r}') \mathrm{d}\boldsymbol{r}\mathrm{d}\boldsymbol{r}' \tag{47}$$

where $\delta\rho = \rho - \tilde{\rho}$. This requires that the projection on the fitting basis of the Coulomb potential due to the true density and that due to the fitted density be equal and leads to a linear equation system for the vector of fitting coefficients $\boldsymbol{d}$:

$$\boldsymbol{A}\boldsymbol{d} = \boldsymbol{v}, \tag{48}$$

where the real, symmetric, and positive-definite matrix $\boldsymbol{A}$ is the representation of the Coulomb interaction in the auxiliary basis, $A_{st} = \langle f_s \| f_t \rangle$. The vector $\boldsymbol{v}$ is the projection of the electrostatic potential on the fitting functions:

$$v_s = \langle f_s \parallel \rho \rangle = \sum_{\mathrm{T}} \sum_{\mu,\nu} I^{(\mathrm{TT})}_{s,\mu\nu} D^{(\mathrm{TT})}_{\mu\nu} \tag{49}$$

where $I^{(\mathrm{TT})}_{s,\mu\nu}$ are the 3-center two-electron repulsion integrals

$$I^{(\mathrm{TT})}_{s,\mu\nu} = \langle f_s \| \rho^{(\mathrm{TT})}_{\mu\nu} \rangle \tag{50}$$

The total Coulomb energy in terms of the fitted density may be expressed simply as:

$$\tilde{E}_J = \tfrac{1}{2}\boldsymbol{d}^{\dagger}\boldsymbol{A}\boldsymbol{d} \tag{51}$$

while the Coulomb matrix elements become

$$\tilde{J}^{(\mathrm{TT})}_{\mu\nu} = \langle \tilde{\rho} \parallel \rho^{(\mathrm{TT})}_{\mu\nu} \rangle = \sum_{t=1}^{N_{\mathrm{aux}}} d_t I^{(\mathrm{TT})}_{t,\mu\nu} \tag{52}$$

The fitting problem is, except for the explicit reference to the large and the small components, identical to that of the non-relativistic case.[142] The formal problem of computing the four-center two-electron repulsion integrals required for the evaluation of the Coulomb matrix is reduced to the calculation of the two-center and three-center two-electron repulsion integrals defining the matrices $\boldsymbol{A}$ and $\boldsymbol{I}^{(\mathrm{TT})}$, respectively. This reduces the formal scaling from $O(N^4)$ to $O(N^3)$ in the evaluation of the Coulomb DKS contribution.

The matrix $\boldsymbol{A}$ may be computed once at the beginning of the self-consistent-field (SCF) iterations, as it does not change from cycle to cycle. The main computational burden in the fitting procedure presented above is the calculation of the vector $\boldsymbol{v}$ and of the fitted matrix elements $\tilde{J}^{(\mathrm{TT})}_{\mu\nu}$. Both these steps require the computation of the three-index matrices $\boldsymbol{I}^{(\mathrm{TT})}$. The vector $\boldsymbol{v}$ is computed efficiently using the Hermite Gaussian density matrix, rather than by applying eqn (49) directly, where the density matrices $\boldsymbol{D}^{(\mathrm{TT})}$ are explicitly involved. This leads to

$$v_s = \sum_{\alpha} \sum_{i,j,k} H_0[\alpha; i, j, k] \langle f_s \parallel \alpha; i, j, k \rangle \tag{53}$$

This approach avoids any explicit reference to the large or small components and exploits all the advantages of using the Hermite density matrix that we have seen in the J-matrix algorithm. The effectiveness of this approach in our scheme is further enhanced by using, as fitting functions, primitive HGTFs that are grouped together in sets sharing the same exponents. The sets are formed so that to an auxiliary function of given angular momentum are associated all the functions of smaller angular momentum. For instance, a d auxiliary function set contains ten primitive Hermite Gaussians, one s, three p, and six d functions all with the same exponent. This scheme allows the efficient use of the recurrence relations[131] of Hermite polynomials in the computation of two-electron integrals. Analogous schemes have been adopted in the non-relativistic DFT code deMon.[148]

We have shown[64] that optimized fitting basis sets can be easily obtained by applying standard basis optimization procedures used in the nonrelativistic context, permitting to achieve fitting accuracies adequate also for heavy atoms. For gold, a small fitting basis which consists of 14 d and 2 g sets (210 HGTFs in total) resulted in a Coulomb energy exact to within 0.1 mhartree per atom. This is the degree of accuracy usually accepted for accurate results on light-atom systems in the nonrelativistic context. Note that a 50% larger fitting basis comprising 2 s, 13 d and 5 g sets (307 HGTFs in total) was enough to reach accuracies below 1 microhartree per atom. The performance and scaling properties of the above approach have been discussed in ref. 64. Compared to the previous standard J-matrix method, calculations using this strategy on gold clusters have exhibited speedups of about two orders of magnitude, increasing with cluster size.

Recently we have further improved the above approach by adopting a fitting scheme making use of the Poisson equation.[67] The basic idea of "Poisson fitting" was first discussed by Mintmire and Dunlap,[144] and then turned into a practical implementation by Manby and Knowles.[66,147] This consists essentially in the adoption of a density expansion scheme written as

$$\tilde{\rho}(\boldsymbol{r}) = \sum_{t=1}^{N_p} c_t \hat{P}\xi_t(\boldsymbol{r}), \tag{54}$$

where $\hat{P} = -(1/4\pi)\nabla^2$ and the ξ_t are a set of N_p suitable auxiliary functions which are supposed to fit the Coulomb potential. If these functions are assumed to have (individually) the correct asymptotic behaviour, the scheme immediately leads to a dramatic simplification of the A matrix elements to

$$A_{st} = \langle \xi_s | \hat{P}\xi_t \rangle = \int \xi_s(\boldsymbol{r}) \hat{P}\xi_t(\boldsymbol{r}) \mathrm{d}\boldsymbol{r} \tag{55}$$

reducing a six-dimensional two-electron repulsion integral to a three-dimensional (kinetic-energy like) one-electron integral. Introducing the same transformation into the three-center integrals simplifies them to one-electron integrals as well:

$$I^{(\mathrm{TT})}_{s,\mu\nu} = \langle \xi_s | \rho^{(\mathrm{TT})}_{\mu\nu} \rangle \tag{56}$$

The efficacy of this approach depends in practice on the accuracy with which the auxiliary functions can fit the Coulomb potential. In this respect, one can easily see that the use of fitting functions that decay faster than any power of $1/r$, such as Gaussians, otherwise the most natural choice, leads to a fitted potential that has an unphysical asymptotic behavior: it turns out that the fitted electron density integrates to a vanishing net charge and has vanishing higher order moments, which is obviously unacceptable.[66,147] The correct long-range behavior of the Coulomb potential is restored by the use of a hybrid fitting procedure, combining both the electrostatic metric and

the Poisson metric.[66] The total electron density is thus cast in the form

$$\tilde{\rho}(\boldsymbol{r}) = \sum_t d_t f_t(\boldsymbol{r}) + \sum_a c_a \hat{P}\xi_a(\boldsymbol{r}), \qquad (57)$$

where the $f_t(\boldsymbol{r})$ are a small number of conventional basis functions, which generate the correct asymptotic behavior of the electrostatic potential and produce its correct multipole moments. The Poisson fitting functions, $\hat{P}\xi_a(\boldsymbol{r})$, are used to adjust the shape of the charge density without altering the long-range features of the potential. Having restored the presence of conventional basis functions in the density fitting procedure, part of the savings afforded by the Poisson procedure are of course lost, the balance depending critically on the number of conventional functions required to satisfactorily fit the density. This question compounds the problem of choosing and optimizing a suitable set of auxiliary Poisson fitting functions, for which much less experience is available in heavy-element relativistic quantum chemistry than in the more conventional non-relativistic domain.

We have proposed a particularly simple and efficient method for the generation of accurate auxiliary basis sets, based on already available standard Coulomb fitting sets. We choose to use directly primitive HGTFs as auxiliary basis functions. As happens in the standard density fitting approach,[149] this brings about many powerful simplifications. The first step thus consists of taking a HGTF fitting basis set optimized over the Coulomb metric and applying the Poisson operator to it. This generates in the simplest way a basis set of Poisson functions. (Note that application of the Laplacian to a HGTF simply yields a sum of HGTFs with higher angular momentum.) In a second stage we add and optimize a small number of HGTF functions in order to achieve a certain fitting accuracy. The approach is simple and fast and requires only the optimization of a few functions. We could indeed show that the number of standard auxiliary functions that need to be added to the Poisson set in order to achieve a fitting accuracy equal to or, in some cases, exceeding that of the standard procedure is extremely small. Further a remarkably high accuracy is preserved both for light and heavy atoms. As an example, in the case of gold we found that the addition of just two *s* and one *f* HGTF sets (22 functions), as standard fitting functions, was sufficient to recover the level of accuracy obtained by the standard fitting.[67] Note that, in this way, the extra optimization effort required by the adoption of the Poisson scheme concerns only three independent parameters, the three unique extra HGTF exponents.

Our implementation of the Poisson fitting scales exactly like the standard fitting procedure with the size of the chemical system under study, but the absolute computational effort is significantly smaller, usually by a factor of two. One crucial property of the Poisson fitting scheme is the band structure of the matrix involved, which originates naturally from the locality of the Coulomb potential generated by the Poisson fitting functions, which decays indeed exponentially. As a consequence, many more integrals are negligibly small compared to the standard fitting procedure. Considering a compact molecular system like $Au(H_2O)_9^+$, screening the integrals at a threshold of 10^{-12} hartree resulted in a total number of integrals to be considered which is about 5% of that of the standard fitting case. In cases such as a linear chain of gold atoms (*e.g.*, Au_{16}), integral evaluation easily approaches the linear scaling regime.

4.3 Density fit for the exchange–correlation matrix

Once the density fitting approach is adopted to compute the Coulomb contribution to the DKS matrix, eqn (52), the computation bottleneck moves to the evaluation of the exchange–correlation matrix. It is therefore desirable to use explicitly the fitted density also in this computation step. The idea of using directly the density expansion obtained from the variational Coulomb fitting into the exchange–correlation functional is relatively old[150,151] and a number of modern effective implementations have been proposed.[149,152] Our own, summarized below, has been described in ref. 68.

The approximated exchange–correlation matrix contribution to the DKS matrix is given by:

$$\tilde{K}^{(\mathrm{TT})}_{\mu\nu} = \frac{\partial E^{(l)}_{\mathrm{xc}}[\tilde{\rho}]}{\partial D^{(\mathrm{TT})}_{\mu\nu}} = \int \frac{\delta E^{(\mathrm{l})}_{\mathrm{xc}}[\tilde{\rho}]}{\delta\tilde{\rho}(\boldsymbol{r})} \frac{\partial\tilde{\rho}(\boldsymbol{r})}{\partial D^{(\mathrm{TT})}_{\mu\nu}} \mathrm{d}\boldsymbol{r} \qquad (58)$$

where the functional derivative defines the exchange–correlation potential, eqn (6), as a functional of the fitted density. Using a fitted electronic density expression such as eqn (46), it follows that the partial derivative of the density with respect to the density matrix elements is given by

$$\frac{\partial\tilde{\rho}(\boldsymbol{r})}{\partial D^{(\mathrm{TT})}_{\mu\nu}} = \sum_t \frac{\partial d_t}{\partial D^{(\mathrm{TT})}_{\mu\nu}} f_t(\boldsymbol{r}) = \sum_{s,t} A^{-1}_{ts} I^{(\mathrm{TT})}_{s,\mu\nu} f_t(\boldsymbol{r}) \qquad (59)$$

where the three-index repulsion integrals of eqn (50) and the inverse Coulomb interaction matrix of the auxiliary set, $\boldsymbol{A}^{-1}$, appear. Introducing eqn (59) in eqn (58) and integrating we obtain an approximated expression for the exchange–correlation matrix elements which has a very simple form:

$$\tilde{K}^{(\mathrm{TT})}_{\mu\nu} = \sum_{s,t} A^{-1}_{ts} w_t I^{(\mathrm{TT})}_{s,\mu\nu} = \sum_s z_s I^{(\mathrm{TT})}_{s,\mu\nu} \qquad (60)$$

with z_t being the elements of the vector solution of the following linear system:

$$\boldsymbol{Az} = \boldsymbol{w} \qquad (61)$$

where the vector $\boldsymbol{w}$ is the projection of the exchange–correlation potential of the fitted density on the fitting functions:

$$w_s = \langle\tilde{v}^{(\mathrm{l})}_{\mathrm{xc}}|f_s\rangle = \int v^{(\mathrm{l})}_{\mathrm{xc}}[\tilde{\rho}(\boldsymbol{r})] f_s(\boldsymbol{r})\mathrm{d}\boldsymbol{r} \qquad (62)$$

An interesting property, easy to show, of this scheme is that exchange–correlation potential obtained, has the same projection onto the true density and onto the fitted one:

$$\langle\rho|\tilde{v}_{\mathrm{xc}}\rangle = \langle\tilde{\rho}|\tilde{v}_{\mathrm{xc}}\rangle \qquad (63)$$

This formalism may be easily extended to include constraints on the fitting procedure, such as the density integrating to the exact number of electrons or higher multipoles.[149]

Once the vectors $\boldsymbol{d}$ and $\boldsymbol{z}$ are available, the Coulomb and exchange–correlation contributions to the DKS matrix can be computed in a single step:

$$\tilde{J}^{(\mathrm{TT})}_{\mu\nu} + \tilde{K}^{(\mathrm{TT})}_{\mu\nu} = \sum_{t=1}^{N_{\mathrm{aux}}} I^{(\mathrm{TT})}_{t,\mu\nu}(d_t + z_t) \qquad (64)$$

The elements of the vector $\boldsymbol{w}$, which involve integrals of the exchange–correlation potential, can be computed numerically by the integration scheme already implemented in the code.[26] It is however important to compute them especially accurately, to minimize error propagation, *via* the solution of the linear system in eqn (61), to the approximate exchange–correlation matrix, eqn (60). In this respect, it is worth noting that very fine integration grids can be adopted and high accuracy enforced without impairing the computational advantages of the method, because the cost of the numerical integration is much reduced compared to the standard procedure. In the latter, the integration step scales as $N^2 \cdot N_g$, where N is the number of G-spinor basis functions and N_g the number of grid points. By contrast, because now the fitted density is a linear combination of N_{aux} auxiliary functions, the numerical integration step scales only as $N_{aux} \cdot N_{grid}$. In addition, in the numerical integration procedure we can now take advantage of the particular choice of auxiliary functions: the use of primitive HGTFs, grouped together in sets sharing the same exponent, reduces the expensive operation of evaluating large numbers of Gaussian exponents at each grid points. Finally, further computational savings arise from the extensive use of the Hermite polynomial recurrence relations for evaluating the angular part of the fitting functions and their derivatives. Benchmark calculations on gold clusters have shown that this global density fitting approach leads to a reduction of the scaling order of the method to less than $N^{2.9}$, with a drop in the pre-factor, compared to the conventional scheme, of over two-orders of magnitude.

An important issue of this global density fitting approach is the accuracy loss in the total energy due to the fact that the density is fitted over the sole Coulomb energy. Different fitting and auxiliary set optimization schemes have been proposed[149,152] and also investigated by us.[68] We have found that the loss of accuracy in the total energy can in fact be controlled and made negligible with a simple scheme. This is based on the observation that the electron density obtained by making the approximate total-energy functional stationary with respect to variations in the orbital spinor coefficients gives, in turn, a total energy that is almost exactly coincident with that obtained with the "exact" density. In other words, the total energy calculated using the converged density in a simple "restart" procedure compensates almost exactly for the use of a fitted density in the Coulomb and exchange–correlation interactions. We refer the reader to ref. 68 for additional details.

4.4 Parallelization strategies

The great algorithmic efficiencies achieved by coupling the global density-fit approach with the underlying G-spinor, HGTF-basis structure of BERTHA leave two big hurdles untouched on the way towards truly large-scale DKS applications: one is the fact that the computational bottleneck is progressively shifted towards the linear algebra operations and, especially, matrix diagonalization; the other, related, problem is the "memory bottleneck": the huge basis sets required for the accurate all-electron treatment of many heavy atoms at once lead to matrix sizes that simply cannot be handled on the typical computer. It seems clear that only a suitably designed data-parallel approach can be of help on both counts. We have tackled this problem in two successive steps, concentrating on the three memory-demanding and time-consuming phases of a DKS calculation: $\boldsymbol{J} + \boldsymbol{K}$ matrix construction, matrix diagonalization, and level-shifting, which involves the double matrix multiplication yielding the DKS matrix in spinor space.

In the first parallel implementation,[69] we adopted a sort of master–slave paradigm which only partially solves the memory bottleneck problem. In this approach one of the concurrent processes, the master, still needs to allocate in fast memory all the entire arrays of a calculation, namely basis overlap, density, DKS and eigenvector matrices, while all processes share the computation burden. In this way, effective memory distribution can only be achieved on advanced parallel systems offering some fast transparent global memory mechanism, such as the SGI NUMAflex architecture[153] available on the SGI Altix 4700 system where we have developed and tested the implementation. In a subsequent modification, still under development and to be only preliminarily discussed here, we have implemented a complete and explicit memory distribution scheme which overcomes these limitations. In both cases, the parallel software tools we have used are the widely available (and often optimized) Message Passing Interface (MPI)[154] and ScaLAPACK libraries.[155]

To parallelize the $\boldsymbol{J} + \boldsymbol{K}$ matrix construction, the most elementary and efficient approach consists in the assignment of matrix blocks to the available processes. The optimal integral evaluation algorithm, exploiting HGTF recurrence relations, naturally induces a matrix block structure dictated by the grouping of G-spinor basis functions in sets characterized by common origin and angular momentum (see also ref. 29). In the original parallel scheme, the master process broadcasts the small $i\boldsymbol{d} + \boldsymbol{z}$ vector appearing in eqn (64) to all the slaves once at the beginning of the computation and then begins to dispatch matrix block computations in an "on-demand" scheme. Each slave process allocates only a local small array where it computes its $\boldsymbol{J} + \boldsymbol{K}$ matrix block, which is then sent back to the master. The latter progressively stores all received blocks in their appropriate location of the global $\boldsymbol{J} + \boldsymbol{K}$ matrix and finally redistributes the whole array according to the so-called two-dimensional block-cyclic decomposition.[155] This step is needed in order to make use of the various ScaLAPACK routines which perform the required matrix operations in parallel, including diagonalization, level-shifting, and density construction. Since the small blocks are not all of the same size, this approach guarantees a good overlap between communication and computation. Furthermore, the fact that each slave computes only a small portion of the $\boldsymbol{J} + \boldsymbol{K}$ matrix at a time guarantees a good cache reuse. After diagonalization and density construction, the eigenvectors and the density matrix are collected on the master. The communications required, both from and towards the master, show a running time that is almost independent from the number of processes involved.[69] A significant computational advantage of the parallel scheme stems from the fact that the ScaLAPACK routines permit the computation of only a subset of eigenvalues and eigenvectors. This is particularly beneficial, in terms of both time and memory requirements, in DKS computations

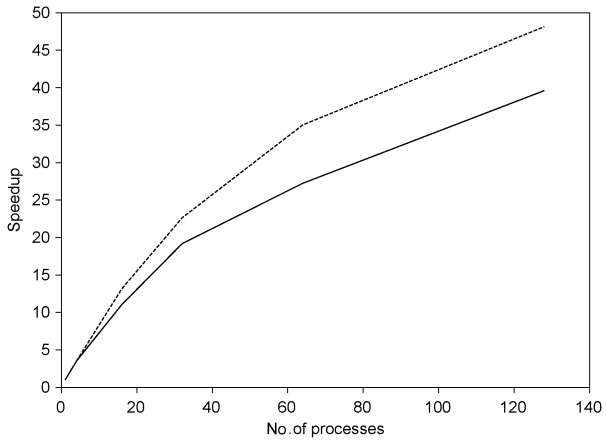

Fig. 1 Speedup obtained in a parallel DKS calculation on a cluster of 32 gold atoms using up to 128 processors (solid line). The upper dashed line shows the theoretical maximum speedup achievable taking into account the unparallelized fraction of the code (Amdhal's law).

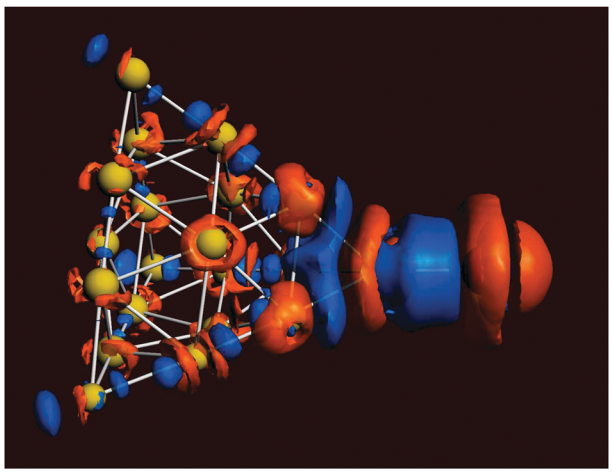

Fig. 2 DKS/BLYP contour plot of the electron density difference upon bond formation between Copernicium and an Au_{20} cluster. Red isodensity surfaces identify zones of density decrease, blue ones of density increase. The density value at the surfaces is $\pm 8 \times 10^{-5}$ e a.u.$^{-3}$.

where only the occupied positive-energy spinors are needed to represent the density, and these constitute only a small fraction of the whole one-particle basis space.

To test the above parallel approach, we performed several computations on various gold clusters.[69] The speedup observed generally tends to increase with the size of the system under study. The $\boldsymbol{J} + \boldsymbol{K}$ matrix construction step scales extremely well for large systems, reaching 95% of the theoretical maximum with 128 processors for Au_{32}. The other phases of the calculation scale less satisfactorily, reflecting the performance limitations of the underlying ScaLAPACK implementation. Fig. 1 displays a plot of the resulting global speedup for the DKS calculation on Au_{32}. The performance appears to converge to more than 82% of the theoretical maximum on 128 processors, and turns out to be about 60% of the limit value for an infinite number of processors (when the execution time reduces to that of the unparallelized portion).

As a further example of the large-scale applications made accessible by our parallel DKS code, we have investigated the absorption of a super-heavy atom, Copernicium (E112), on a Au_{20} cluster. This kind of processes is important to establish, both by experiment and theoretically, the nature and properties of these exotic chemical elements.[156] We have used a large G-spinor basis set whose large component is a decontraction of Dyall's triple-zeta quality basis for both gold and E112.[157,158] The corresponding small-component basis was generated using the restricted kinetic balance relation. This results in a DKS matrix of dimension 24 584 (9 GB double-precision complex numbers). The density functional used is the Becke 1988 exchange functional (B88)[159] plus the Lee–Yang–Parr (LYP) correlation functional[160] (BLYP). The calculation has been carried out with a total energy convergence threshold of 10^{-7} hartree, on the SGI Altix 4700 mentioned above, using 64 processors. A SCF cycle takes about 67 minutes and the full procedure was found to converge in twenty cycles. This means that the full four-component DKS calculation for this large system, treating explicitly its 1692 electrons, took about 22 hours.[161]

A qualitative insight into the nature of the Au_{20}–Cn interaction is provided by the analysis of the electronic density difference between the complex and the non-interacting fragments placed at the same geometry. A 3D contour plot of this difference is shown in Fig. 2. A surprising feature is its very rich and complex structure, with the density rearrangement delocalized over the whole Au cluster and reaching its most remote regions far away from the interaction zone. Another quite remarkable general feature (not immediately visible in the figure) is that the valence electron rearrangement upon bond formation has large repercussions in the core-electron region closer to the nuclei. The density accumulation is particularly pronounced in the Cn–Au internuclear region and in the zone between the first two gold layers (*i.e.*, between the gold atom bound to E112 and the three neighbors below it). Some density depletion zone is observed instead on the far side of Cn, opposite to the Cn–Au bond. The results of these investigations, whose details will be given in a forthcoming paper, have suggested that Copernicium possesses a marked chemical inertia, akin to that of a noble gas.

As mentioned earlier, we conclude this section with a brief presentation of an explicit data-parallel approach to the G-spinor DKS method, whose details and performance will be the subject of a forthcoming paper.[162] Here each process performs an identical computation, and there is no distinction between master and slaves. The DKS arrays are always explicitly distributed among all processes and there is no need for a single global allocation. This also mean that, in the $\boldsymbol{J} + \boldsymbol{K}$ matrix construction, no process is lost to the task of coordinating the workload, which is a non-negligible gain in case only few processes are available.

The entire procedure can be summarized as follows. Each concurrent process computes an evenly balanced subset of DKS matrix blocks, and stores the result in a local array. At the end of the procedure the matrix is thus automatically distributed among all the processes, in accord with the matrix block structure dictated by the grouping of G-spinor basis functions (see above). Now the matrix needs to be re-distributed according to the two-dimensional block cyclic distribution used by ScaLAPACK and, to efficiently perform this task, we implemented

Table 1 $\boldsymbol{J} + \boldsymbol{K}$ matrix construction speedup for the master–slave (MS) and data-parallel (DP) approaches. All tests have been carried on an IBM-SP6. The concurrent processes used are shown as the logical two-dimensional grid, $n \times m$, "seen" by ScaLAPACK

		Processor grid				
Cluster	Parallel scheme	2 × 2	4 × 4	4 × 8	8 × 8	8 × 16
Au_2	MS	2.9	10.2	14.6	27.5	27.5
	DP	3.8	9.7	14.5	23.3	21.1
Au_4	MS	3.0	13.3	24.3	36.2	55.8
	DP	3.9	14.4	23.7	33.1	46.3
Au_8	MS	3.0	14.8	30.8	63.8	117.7
	DP	3.9	15.6	31.9	63.7	103.9
Au_{16}	MS	3.0	15.0	31.5	62.8	124.2
	DP	4.0	16.1	32.4	63.8	123.8

a dedicated routine mapping the two distribution patterns.[162] This explicit matrix distribution and the effective computation parallelism make the applicability range of the code essentially "open-ended" and, most of all, essentially portable on any parallel architecture including low-cost clusters. Some very preliminary tests have been carried out on an IBM SP Power 6.

We performed several computations with up to 128 concurrent processes for different gold clusters from Au_2 to Au_{16}, representing a testing ground for a wide range of memory requirements and double-precision complex array handling conditions: the DKS matrix sizes ranged from 1560 for Au_2 (37.1 MB) to 12 480 for Au_{16} (2.3 GB). In Table 1 we show the speedup of the $\boldsymbol{J} + \boldsymbol{K}$ matrix construction step for both the master–slave approach and the new data-parallel one. Note that the available processes are mapped, in the ScaLAPACK model, onto a two-dimensional rectangular grid, and performance may depend, even substantially, on the grid shape.[163] The results show, as discussed above, that the data-parallel approach wins when using few processes. When the number of processors grows, the master–slave model performs slightly better. This must be expected because in the data-parallel scheme a price is paid to carry out the array re-distribution mapping integral evaluation parallelism with block-cyclic decomposition. This operation shows a dependence of the communication time on the number of processes.[162] However, the parallel efficiency of both approaches turns out to be excellent and comparable (about 97% with 128 processors), which clearly makes the data-parallel scheme preferable in terms of memory management.

Because of the good data-parallel performance of the code, an interesting further development worth exploring is its porting on a GP-GPU (General-Purpose computation on Graphics Processing Units) architecture.[164] This solution may be cost-effective for moderate-size systems by easily replacing the ScaLAPACK calls with the equivalent CUBLAS[165] and CULA[166] ones.

5 Time-dependent electromagnetic interactions

The circumstances under which relativistic description of the interaction between an atomic or molecular electron and an external electromagnetic field is required are usually associated with two critical physical conditions.[167–170] In the first of these, the intensity of the incident electromagnetic pulse is so large that an electron acquires a relativistic ponderomotive energy, which is the kinetic energy that a free electron acquires by multiphoton absorption. This requires a relativistic description of its charge–current density once it is liberated from the atom into the continuum. Conventionally, this condition is regarded as giving rise to so-called 'non-dipole' or 'magnetic' interactions because the interaction potential exhibits a non-trivial spatial variation. In the second circumstance, the bound-states of the atom require a relativistic description by virtue of the strength of the nuclear Coulomb field.[171] In a relativistic description based on the Dirac equation, however, we may unify these apparently distinct experimental conditions within a common formalism by noting that both the external electromagnetic field and the nuclear Coulomb field may be treated on the same footing by adopting a covariant description of the complete electromagnetic four-potential, $A^{\mu}(x)$, where x denotes the space-time four-vector, $x = (ct,\boldsymbol{r})$.

In this section, we discuss the formulation and phenomenology of relativistic and magnetic effects in strong-field electromagnetic interactions involving one-electron systems. This forms the foundation for the subsequent section, which develops the implementation of a relativistic time-dependent density-functional formalism of complex, many-body systems. For greater clarity, in the formulae of this section, we explicitly include the electron charge—e and mass m.

The Lorentz-invariant scalar quantity, η, is defined by[169,172]

$$\eta = k_{\mu}x^{\mu} = \omega t - \boldsymbol{k}\cdot\boldsymbol{r} \tag{65}$$

where ω is the angular frequency and $\boldsymbol{k}$ is the wave-vector of the external electromagnetic field. The vector potential of the electromagnetic field is then $\boldsymbol{A}(\eta)$ in terms of which the electric field, $\boldsymbol{E}(\eta)$, and magnetic field, $\boldsymbol{B}(\eta)$, are given by

$$\boldsymbol{E}(\eta) = -\frac{\partial \boldsymbol{A}(\eta)}{\partial t} \tag{66}$$

$$\boldsymbol{B}(\eta) = \nabla \times \boldsymbol{A}(\eta). \tag{67}$$

Assuming the Coulomb gauge condition fixes the nuclear potential to act as a diagonal time-independent scalar operator, $V(\boldsymbol{r})$, and the vector potential, $\boldsymbol{A}$, which has both spatial and temporal variation, to be perpendicular to $\boldsymbol{k}$. We will consider the specific case of a laser pulse of angular frequency ω propagating in the z-direction and polarized in the x-direction, we have $\boldsymbol{k} = k\hat{\boldsymbol{z}}$, where $k = \omega/c$ and $\hat{\boldsymbol{z}}$ is a unit vector in the z-direction. Then

$$\boldsymbol{E}(\eta) = E(\eta)\hat{\boldsymbol{x}} \tag{68}$$

$$\boldsymbol{B}(\eta) = B(\eta)\hat{\boldsymbol{y}} \tag{69}$$

where $\hat{\boldsymbol{x}}$ and $\hat{\boldsymbol{y}}$ are, respectively, unit vectors in the x- and y-directions and $E(\eta)$ and $B(\eta)$ define, respectively, the electric and magnetic field amplitudes.

Much of the phenomenology of these strong-field interactions may be deduced by considering the classical Lorentz equation for an electron in this linearly-polarized field. This is given by

$$\frac{\mathrm{d}\boldsymbol{p}}{\mathrm{d}t} = -e[\boldsymbol{E}(\eta) + \boldsymbol{v} \times \boldsymbol{B}(\eta)] \tag{70}$$

where $\boldsymbol{p} = \gamma m\boldsymbol{v}$, $\gamma = \sqrt{(1-\beta^2)}$, $\beta = v/c$ and v is the magnitude of the electron velocity, $\boldsymbol{v}$.

If terms to order $1/c$ are retained, the electronic motion is two dimensional in the xz-plane, with

$$\frac{\mathrm{d}v_x}{\mathrm{d}t} = -E(\omega t) \tag{71}$$

$$\frac{\mathrm{d}v_z}{\mathrm{d}t} = -v_x B(\omega t) \tag{72}$$

To this order in $1/c$, therefore, the interaction with the fields is dipolar, since any spatial dependences of the field amplitudes $E(\eta)$ and $B(\eta)$ do not appear. The presence of the magnetic field has no influence on motion in the polarization direction, which is driven entirely by the time-variation in the electric field, which is the dominant contribution.

If we assume that the electron is initially at rest at the coordinate origin, the displacements of its position are given by

$$x(t) = \int_{-\infty}^{t} A(\omega\tau)\mathrm{d}\tau \tag{73}$$

$$z(t) = \frac{1}{2c}\int_{-\infty}^{t} v_x^2(\tau)\mathrm{d}\tau. \tag{74}$$

The motion of the electron in the x-direction generally follows the time-dependence of the electric field. In the presence of a time-dependent magnetic field, however, the effect is always to cause the electron position to drift in the positive z-direction. In the particular case of a pulse arriving at $t = 0$ with a step-function profile of amplitude E_0, $x(t)$ and $z(t)$ possess the explicit functional forms

$$x(t) = \frac{E_0}{\omega^2}\sin(\omega t) \tag{75}$$

$$z(t) = \frac{E_0^2}{2c\omega^2}\left[\frac{t}{2} + \frac{\sin(2\omega t)}{4\omega}\right] \tag{76}$$

The drift in the z-direction per optical cycle is given by $\pi E_0^2/2c\omega^3$ bohr, which may be used to identify the regime of interaction parameters for which magnetic effects are important. At optical wavelengths, the critical incident laser intensity is generally regarded to be approximately 1×10^{15} W cm^{-2}.[171] For intensities less than this value, one may ignore the effects of the magnetic interaction and adopt a description based on the electric dipole approximation.

Field-induced relativistic effects are important in strong-field electron-laser interactions if the ponderomotive energy, U_p, is of the order of the rest-mass energy. A convenient measure of this circumstance is the q-parameter, defined in atomic units by $q = U_\mathrm{p}/c^2$, which is given explicitly by

$$q = \frac{E_0^2}{4\omega c^2}. \tag{77}$$

Relativistic effects arising from the variation in electron mass with speed are significant whenever q approaches or exceeds unity. Under these circumstances, it has been shown that the relativistic electron propagates in the field with an effective mass, m^*, where

$$m^* = m\sqrt{1+2q} \tag{78}$$

where m is its rest mass.

It is generally agreed that relativistic effects are significant in systems for which the effective Coulomb field experienced by the electron exceeds approximately ten.[171] But it is also the case that a more convenient and unified representation of the bound-state electronic structure may be obtained if we adopt a formulation based on the Dirac equation whenever the atomic or molecular system contains heavy elements. Multiphoton ionization from heavy elements may involve a number of channels made available by spin–orbit coupling, which may be absorbed within a Dirac four-spinor description. In our formulation, we examine a formulation based on Dirac four-component spinors which are coupled to the four-vector components of the electromagnetic field. This facilitates a unified treatment of relativistic, electric and magnetic effects in atoms and molecules, containing heavy or light elements interacting with strong electromagnetic pulses.

It is well-known[173] that the dynamics of non-relativistic hydrogenic systems are subject to a trivial scaling of $\boldsymbol{r}$ and t that provides a description of all such systems. The relations that rescale the non-relativistic time-independent hamiltonian are, respectively,

$$\boldsymbol{r}' = Z\boldsymbol{r}$$

$$t' = Z^2 t,$$

where Z is the nuclear charge. These scaling laws may be used, for example, to establish the Z-independence of the dipole polarizability of hydrogenic atoms. The scaling of time-dependent phenomena is preserved if the applied electric field strength, E_0, and the central frequency of the field, ω_0, are also scaled by the relations

$$E_0' = E_0/Z^3 \tag{79}$$

$$\omega_0' = \omega_0/Z^2. \tag{80}$$

These scaling laws do not apply to any formulation based on the Dirac equation, except in the non-relativistic limit, $c \to \infty$. Any deviation from these non-relativistic scaling relations indicates either a relativistic effect, whose origin may primarily be attributed to the state-dependent variation of mass with velocity, or a magnetic effect arising because the dipole approximation is no longer valid.

5.1 Formulation

We assume that a solution exists of the time-dependent Dirac equation,

$$\hat{H}_\mathrm{D}(x)\boldsymbol{\Psi}(t) = i\frac{\partial\boldsymbol{\Psi}(t)}{\partial t} \tag{81}$$

where we restrict our attention to Dirac operators of the form

$$\hat{H}_\mathrm{D}(x) = \{c\boldsymbol{\alpha}\cdot[\hat{\boldsymbol{p}} + e\boldsymbol{A}(\eta)] + V(\boldsymbol{r}) + c^2\boldsymbol{\beta}\}. \tag{82}$$

It is further assumed that one can define a complete set of single-particle four-spinors, $\{\boldsymbol{\psi}_k(\boldsymbol{r})\}$, that are solutions of a

model time-independent Dirac equation. The required time-dependent four-spinor solution of the time-dependent Dirac equation is expanded in this basis as

$$\boldsymbol{\Psi}(t) = \sum_k c_k(t)\boldsymbol{\psi}_k(\boldsymbol{r})\exp(-iE_k t) \tag{83}$$

where E_k is the single-particle eigenvalue associated with $\{\boldsymbol{\psi}_k(\boldsymbol{r})\}$ and $c_k(t)$ is an expansion coefficient. If the $\boldsymbol{\psi}_k$ are eigenfunctions of $\hat{H}_{\mathrm{D}}(x)$, eqn (82), with $\boldsymbol{A}(\eta) = 0$, the expansion coefficients may be found as solutions of an infinite set of coupled differential equations of the form

$$\frac{\partial c_n}{\partial t} = -i\sum_k \langle n|ec\boldsymbol{\alpha}\cdot\boldsymbol{A}(\eta)|k\rangle \exp(i\omega_{nk}t)c_k(t) \tag{84}$$

where $\omega_{nk} = (E_n - E_k)$.

The relativistic formulation for the construction of a time-dependent wavefunction from a complete basis of single-particle solutions of a time-independent model problem follows closely the apparent practices of non-relativistic theory. There exists, however, a critical difference in the relativistic case that introduces new features into the solution for the expansion coefficients, $\{c_k(t)\}$. For any typical atomic or molecular potential, the solutions of the model, time-independent Dirac equation may be classified as falling into one of two classes. The so-called positive-energy solutions all satisfy the condition $E_k > 0$, on a scale for which the rest-mass energy of the electron is mc^2 a.u. These solutions contain all of the states that map onto the non-relativistic spin-orbital solutions of the Schrödinger equation in the formal limit $c \rightarrow \infty$. A second class of solution occurs for $E_k < -mc^2$ a.u., which are known as the 'negative-energy' solutions. From a mathematical point of view, only the union of these two classes of solutions forms a complete set, and so one may not arbitrarily exclude the negative-energy states from the sum over the index k in eqn (83). The role of the negative-energy states is further complicated by the realization that definition of the two classes of solutions depends on the specification of the time-independent potential that is used to generate them. Since the union of the two classes forms a complete set, it follows immediately that a negative-energy state in one representation will have a non-vanishing projection onto a positive energy solution corresponding to a different time-independent potential.

The critical field strength to produce real electron–positron pairs is $E_{\mathrm{crit}} = m^2c^3/e \simeq 3 \times 10^6$ a.u., and typically we will be interested in much lower applied fields than this. The time-dependence of the applied electromagnetic four-potential *necessarily* involves, however, a unitary mixing between the positive- and negative-branches of the spectrum generated for a single, time-independent potential. Physically, the negative-energy solutions are assumed to be filled with electrons in a manner consistent with the Pauli-exclusion principle. The mixing of positive and negative energy states through the action of an external electromagnetic field has the effect of producing a polarization potential through the creation of *virtual* electron–positron pairs.

The effect of this is that what one describes as a negative- or positive energy state has meaning only when qualified by reference to the potential that generated the elements of the spectrum. Any applied field will cause the positive- and negative-energy states of the free-electron Dirac equation to mix. The $1s_{1/2}$ ground state spinor contains both positive- and negative-energy free-electron components. But if we dress the states with the instantaneous potential, we may exclude contributions from negative-energy states, simply because they have negligible interaction with the current Dirac four-spinor. These are both valid representations of the electronic state of the system, but they represent different frames of reference. The physical interpretation differs between these representations because they start from distinct representations of the states with respect to which the system is propagating in time.

An additional physical feature of the solution of the time-dependent Dirac equation arises if we compare the use of eqn (81 and 82) with the non-relativistic velocity-gauge form of the non-relativistic time-dependent Schrödinger equation,

$$i\frac{\partial \boldsymbol{\Psi}^{\mathrm{NR}}}{\partial t} = \left[-\frac{1}{2}\nabla^2 + V(\boldsymbol{r}) + \frac{e}{m}\boldsymbol{A}(\eta)\cdot\boldsymbol{p} + \frac{e^2}{2m}A^2(\eta)\right]\boldsymbol{\Psi}^{\mathrm{NR}}. \tag{85}$$

The Dirac equation manifests treat the electron–positron field and the electromagnetic field on the same footing, because $\boldsymbol{p}$ and $\boldsymbol{A}(\eta)$ appear together as linear operators in eqn (82). The interaction between the vector potential is coupled through the relativistic operator, $\boldsymbol{\alpha}$, which gives the field access to the electronic spin variables. In the Schrödinger equation, however, the vector potential appears as both a linear and a quadratic operator, which are interpreted conventionally as giving rise to paramagnetic and diamagnetic interactions. In strong-field interactions, it is actually the diamagnetic contribution that dominates, in which the electric component of the external field accelerates an electron, generating a charge–current density that interacts with the magnetic component of the same field. In a relativistic formulation, there is no distinction between paramagnetic and diamagnetic interactions; they are treated on the same footing by the linear interaction hamiltonian, $H_{\mathrm{int}} = ec\boldsymbol{\alpha}\cdot\boldsymbol{A}(\eta)$, which is constructed from the operators α and $\boldsymbol{A}(\eta)$, which act on the space of Dirac four-spinors, rather than the two-component space of non-relativistic spin-orbitals.

5.2 Implementation

There exist two general approaches to the implementation of a time-propagation formalism involving either the time-dependent Schrödinger or Dirac equations. We have already encountered the first of these, in which one first generates a finite-dimensional representation of the complete spectrum for some time-independent model potential, eqn (84). The design of basis sets to perform this task has led to the use of a number of finite basis set representations of Dirac spinors in atomic and molecular electronic structure and many-body theory. The presentation by Selstø *et al.*[172] employed the finite-difference basis set devised by Salomonson and Öster[174] (see also the works of Stacey[175] and Johnson *et al.*[176]).

In this state, time-independent radial solutions of the Dirac equation for a central field are generated on a discrete grid, with radial points, r_i, that are distributed exponentially according to $r_i = r_0\exp(x_i)$, where x_i are specified on a linear grid. This generates a compact representation of the bound-states and low-lying continuum states, but its use is not consistent with

the usual practices of non-relativistic dynamical studies, which tend to discretize space on a dense, linear grid. The reason that this latter grid is chosen is that the interaction of an intense external field with an atom generates wavepackets of arbitrary shape that propagate in the field. In order to obtain either the above-threshold photoelectron spectrum or the radiation field generated by these wavepackets, it is essential that the time-dependent wavefunction be sampled on a grid that is sufficiently dense that it is able to represent each of its relevant Fourier components. The exponential grid generates a rather course grid at large distances from the nucleus and a very dense grid at small radial distances that gives an unbalanced representation of the propagating wavepacket. Although it seems counter-intuitive to disregard the conventional practices of relativistic *bound-state* atomic physics and the established success of the Salomonson and Öster model, the use of a dense linearly-spaced grid is likely to offer an implementation that is more favorable for accurate time-dependent models of highly energetic systems. Equivalently, one may adopt an analytic basis set of *L*-spinors or *G*-spinors or a numerical basis generated from *B*-spline representations of the four-component spinors.[2] Once the basis set has been selected, the implementation depends only on the evaluation of interaction matrix elements and the determination of the expansion coefficients, $\{c_k(t)\}$, in eqn (83). Selstø *et al.*[172] refine this treatment by the further use of a complex coordinate rotation. This is just a numerical device to suppress effects arising from the finite extent of the discretization grid and does not affect the physical interpretation. One may also employ absorbing masks or complex absorbing potentials to eliminate reflections arising from the propagation of the electron to the outer surface of the discretization grid.

A close examination of eqn (84) provides clear indications of the likely origin of numerical problems using finite basis set expansions. We assume that the determination of $\{c_k(t)\}$ proceeds from an initial condition in which $c_0(t) = 1$, where $c_0(t)$ denotes the time-dependent expansion coefficient of the ground state. For convenience, the label k is assumed to take positive integer values when it refers to positive-energy states, and negative integer values for negative-energy states. In the velocity gauge, the magnitudes of the interaction matrix elements $\langle k|H_{\rm int}|0\rangle$ depend rather markedly on whether k refers to a positive- or negative-energy state, because of the off-diagonal nature of the Dirac matrix operator, $\boldsymbol{\alpha}$. The magnitudes of the large and small component functions for a positive-energy state appear with the approximate weights of *unity* and $1/c$, respectively; these weights are reversed for a negative-energy state. Consequently $\langle k|H_{\rm int}|0\rangle$ is approximately a factor of c times larger if k denotes a negative-energy state than if it denotes a positive-energy state. The initial growth in the population of negative energy states is not, therefore, suppressed by the smallness of their interaction matrix elements involving the ground state but, rather, by the highly oscillatory nature of the harmonic factor $\exp(i\omega_{k0}t)$ that appears in eqn (84). If k denotes a negative energy state, ω_{k0} has a numerical value of approximately c^2 a.u. Given that the atomic unit of time corresponds to approximately 2.4×10^{-17} s, the effective coupling between the ground-state coefficient and that of a negative-energy state oscillates approximately 3.5×10^4 times more rapidly than the corresponding quantities involving the ground state and a positive-energy state. This oscillation is so rapid that, irrespective of the numerical procedure used to employ $\{c_k(t)\}$, the populations of the negative energy states never acquire values that approach unity. The largest part of the population transferred from the ground-state is to states of positive-energy, because the most likely outcome of the interaction is to cause above-threshold photoionization, especially for intense, low-frequency incident fields.

This is not intended to suggest, however, that the interactions involving the negative-energy states may be neglected, or that the fact that they cause small corrections means that they are easy to handle numerically. As Selstø *et al.* demonstrate by direct numerical example, neglect of the negative-energy states fails to recover correct results in the non-relativistic limit. The negative-energy states play a crucial role in recovering the contribution to dynamics that is captured in the non-relativistic approximation by the diamagnetic interaction, $e^2A^2(\eta)/2m$. This is a result that has far-ranging consequences that have been noted in the past, notably by Dirac, Furry and Feynman, in the relativistic calculation of Thomson scattering processes.[177] For recent works on the subject see ref. 178 and 179. The fundamental difficulty is that the time-evolution of $c_k(t)$ involves couplings that oscillate on vastly different time-scales, depending on whether k refers to a positive- or negative-energy state. Selstø *et al.*[172] determined the set $\{c_k(t)\}$ by solving eqn (84) as a set of coupled first-order differential equations, using the adaptive-step Runge–Kutta scheme. As those authors state correctly, this has the advantage that it "must" work, provided that one is willing to adopt a sufficiently small step-length in time. These differential equations are regarded, therefore, as "stiff", in the sense that one is forced to adopt a temporal step-length that is dictated by the interaction with negative-energy states; this step-length is of order 10^4 times smaller than that required for non-relativistic calculations, or relativistic calculations that arbitrarily exclude negative-energy interactions.

Rather than adopting a finite-difference approach, such as the Runge–Kutta scheme, to the determination of $\{c_k(t)\}$, one may adopt a unitary evolution scheme. A formal solution to the propagation equation for the expansion coefficients for short time-intervals, δt, is given by

$$\boldsymbol{c}(t + \delta t) = \exp[-i\boldsymbol{H}(t + \delta t/2)\delta t]\boldsymbol{c}(t) \qquad (86)$$

where $\boldsymbol{c}(t)$ is a vector containing the coefficients, $\{c_k(t)\}$ and $\boldsymbol{H}_{\rm D}(t + \delta t/2)$ is the matrix representation of the time-dependent Dirac operator, $\hat{H}_{\rm D}(t)$, evaluated at the midpoint of the propagation step, $t + \delta t/2$. This exponential matrix operator may be evaluated directly, by transforming to a basis in which $\boldsymbol{H}_{\rm D}(t + \delta t/2)$ is diagonal. Alternatively, it may be approximated by the split-operator technique, in which $\boldsymbol{H}_{\rm D}(t)$ is partitioned into a time-independent part, $H^0_{\rm D}$, and a time-dependent remainder, $\hat{H}'(t)$. The time-evolution is then accomplished according to the procedure

$$\begin{aligned}\boldsymbol{c}(t + \delta t) = {} & \exp[-i\boldsymbol{H}'(t + \delta t/2)\delta t/2] \times \exp[-i\boldsymbol{H}^0_{\rm D}\delta t] \\ & \times \exp[-i\boldsymbol{H}'(t + \delta t/2)\delta t/2]\boldsymbol{c}(t). \qquad (87)\end{aligned}$$

This approach has the distinct advantage that the most rapidly-varying part of the calculation is in diagonal form,

since $\exp[-i\boldsymbol{H}^0_{\mathrm{D}}\delta t]$ is, a spinor basis, a diagonal matrix whose diagonal elements are simply $\exp[-iE_k\delta t]$, where $\{E_k\}$ are the set of eigenvalues of $\hat{H}^0_{\mathrm{D}}$. The remaining terms are readily evaluated either by diagonalizing $\boldsymbol{H}'(t + \delta t/2)$, or by noting that the $\boldsymbol{H}'(t + \delta t/2)$ is a sparse matrix, facilitating the evaluation of the matrix exponential in a term-by-term expansion. This approach does not eliminate the need to adopt a very small step length, δt, but it does ensure the unitarity of the propagation at every step.

Selstø *et al.*[172] also consider how a change of gauge suppresses the effects arising from negative-energy states. In particular, the application of the gauge transformation

$$UH_{\mathrm{D}}U^{\dagger} + i\frac{\partial U}{\partial t}U^{\dagger} \tag{88}$$

with the unitary transformation

$$U = \exp(ie\boldsymbol{A}\cdot\boldsymbol{r}) \tag{89}$$

may be employed to replace the velocity gauge interaction, $H_{\mathrm{int}} = ec\boldsymbol{\alpha}\cdot\boldsymbol{A}$, by the length gauge interaction

$$H_{\mathrm{int}} = e\boldsymbol{r}\cdot\boldsymbol{E} + ec(\boldsymbol{\alpha}\cdot\boldsymbol{k})\left(\boldsymbol{r}\cdot\frac{\mathrm{d}\boldsymbol{A}}{\mathrm{d}\eta}\right). \tag{90}$$

It is comprised of a diagonal electric field interaction, identical in form to the non-relativistic electric dipole interaction, and a non-diagonal interaction that is proportional to the magnetic field strength. It is shown that the first term dominates, and that the second contributes only at the level of relativistic corrections of order $1/c^2$. Consequently one may retain just the first term, which strongly suppresses negative energy states and restores the general numerical behaviour to that of the non-relativistic formulation, which utilizes the same interaction.

This transformation restores the numerical characteristics of the solution of the time-dependent Dirac equation to those resembling non-relativistic behaviour, since the dipole interaction matrix elements and excitation energies involving positive-energy states now differ by only small relativistic corrections. Unfortunately, however, the use of the length gauge introduces a new problem that occurs in both the relativistic and non-relativistic formulations. It is well known that if one expands the non-relativistic $\boldsymbol{\Psi}(t)$ in an angular momentum basis,

$$\boldsymbol{\Psi}(t) = \sum_{\ell,m} f_{\ell,m}(r,t)\,Y^m_{\ell}(\vartheta,\varphi) \tag{91}$$

where $f_{\ell,m}(r,t)$ are time-dependent radial functions and $Y^m_{\ell}(\vartheta,\varphi)$ is a spherical harmonic function, its convergence with respect to the orbital angular momentum parameter, ℓ, is *much* faster in the velocity gauge than in the length gauge. This is because the construction of $\boldsymbol{\Psi}(t)$ in the length gauge involves an explicit, numerical construction of the highly-oscillatory gauge transformation, eqn (89). While this is of no physical significance, it is of great practical importance, since the number of terms in eqn (91) becomes prohibitive in the length gauge; it is for this reason that high-precision calculations based on the time-dependent Schrödinger equation are invariably performed in the velocity gauge. This point is also acknowledged by Selstø *et al.*, who note that the maximum value of ℓ to achieve a given accuracy is gauge-dependent.

The recommendation of the study in ref. 172 is that one minimizes the contributions from the highly oscillatory contributions that arise from the negative-energy states by rediagonalizing the representation to redefine the elements of the positive- and negative-energy branches of the spectrum. While oscillatory factors will still occur, the rediagonalization of the representation effectively redefines the instantaneous population to be entirely positive-energy in character. This eliminates couplings between the branches and greatly improves the convergence characteristics of the time-propagation. This advantage does come at some cost, however, because the dimension of the fully-coupled representation becomes prohibitively large if more than about ten angular momentum contributions are included in the basis set.

Rather than employing a basis set expansion, one may instead formulate a practical numerical scheme that more closely resembles the common practices of non-relativistic time-dependent Schrödinger theory. In a relativistic formulation,

$$\boldsymbol{\Psi}(t) = \sum_{\kappa,m}\begin{bmatrix} P_{\kappa,m}(r,t)\chi_{\kappa,m}(\vartheta,\varphi) \\ iQ_{\kappa,m}(r,t)\chi_{-\kappa,m}(\vartheta,\varphi)\end{bmatrix} \tag{92}$$

where $P_{\kappa,m}(r,t)$ and $Q_{\kappa,m}(r,t)$ are, respectively, large and small-component radial spinors characterized by fine-structure labels (κ,m), and $\chi^m_{\pm\kappa}(\vartheta,\varphi)$ are two-component spin-angular functions as in eqn (17)–(18).

The time-evolution operator is now written in configuration-space, rather than in the Hilbert space of a particular basis of time-independent spinors, so that

$$\boldsymbol{\Psi}(t + \delta t) = \exp(-iH_{\mathrm{D}}(t)\delta t)\boldsymbol{\Psi}(t). \tag{93}$$

Following non-relativistic practice (see ref. 180 and references therein), the unitarity of the propagation is maintained by transforming this relationship into an implicit dependence, so that

$$\exp(iH_{\mathrm{D}}(t + 3\delta t/4)\delta t/2)\boldsymbol{\Psi}(t + \delta t) = \exp(-iH_{\mathrm{D}}(t + \delta t/4)\delta t/2)\boldsymbol{\Psi}(t). \tag{94}$$

This implicitly links the back-propagation of the unknown wavefunction, $\boldsymbol{\Psi}(t + \delta t)$, by $\delta t/2$ and the forward propagation of the known wavefunction, $\boldsymbol{\Psi}(t)$, by $\delta t/2$, also by $\delta t/2$. The time-dependent hamiltonians are evaluated at the appropriate time for the midpoint to apply in each propagation step. Expanding the exponential operators and retaining the leading terms yields a relativistic application of the Crank–Nicholson equations

$$[1 + i\hat{H}(t + 3\delta t/4)\delta t/2]\boldsymbol{\Psi}(t + \delta t) = [1 - i\hat{H}(t + \delta t/4)\delta t/2]\boldsymbol{\Psi}(t). \tag{95}$$

In non-relativistic theory, the radial functions $f_{\ell,m}(r,t)$ that appear in eqn (91) are generated on linearly-spaced radial grids, so that they are able to represent highly energetic free-electron wavepackets. The hamiltonian operators then appear as finite-difference representations of the kinetic and potential operators. Regarding the tabulated values of the wavefunction as the elements of a vector, the hamiltonian operators that appear in eqn (95) may be written as square matrices, with diagonal sub-blocks associated with the time-independent part

of the operator and the off-diagonal blocks representing interaction.

It was shown by Salomonson and Öster[174] how valid finite-difference representations of Dirac operators may be constructed, emphasizing how the selection of the radial grid plays a particularly critical role in maintaining the proper separation between positive and negative energy states, and the correct distinction between upper and lower components. Although their analysis was intended mainly to generate spectral representations by diagonalization of the matrix representations of the Dirac operator, their formulation may be used here without significant modification to generate a stable propagation kernel with numerical characteristics reminiscent of the non-relativistic formalism. The critical observation that they made was that functions $P_{\kappa,m}(r,t)$ and $Q_{\kappa,m}(r,t)$ must be discretized on separate, *alternatively interleaved* radial grids, in order that the conventional finite difference representation of the kinetic energy operator be recovered in the non-relativistic limit. We need not follow their complete program here, since they formulated their procedure in order to produce a dense, exponentially weighted grid appropriate mainly for bound-state functions. It is necessary only to follow the preliminary part of their presentation, in which a regularly spaced radial grid is considered. The conventional central-difference formula is adopted for the first-derivative operator, so that, for example,

$$\left[\frac{\mathrm{d}}{\mathrm{d}r}+\frac{\kappa}{r}\right]P(r_{2i},t)\simeq\frac{P(r_{2i+21},t)-P(r_{2i-2},t)}{4h}+\frac{\kappa}{r_{2i}}P(r_{2i},t). \tag{96}$$

In this formulation, the function $P(r,t)$ is tabulated on even-numbered grid points and $Q(r,t)$ on the odd-numbered grid points, which are uniformly spaced with interval h and generated by the labelling scheme $1 \leq i \leq N$. The interval between $P(r_{2i},t)$ and $P(r_{2i+2},t)$ or $Q(r_{2i-1},t)$ and $Q(r_{2i+1},t)$ is, consequently, $2h$.

The right-hand side of eqn (95) may be regarded as the product between a sparse matrix that is blocked by the symmetry labels (κ,m) and a vector containing the known radial amplitudes at time t. The result is a vector. The left-hand side represents the product between another large, sparse matrix, the elements of which are known, and a vector containing the unknown amplitudes at time $t + \delta t$. We may regard eqn (95), therefore, as defining a large system of simultaneous equations of the form $\boldsymbol{Tx} = \boldsymbol{b}$, in which $\boldsymbol{T}$ is sparse and, critically, the matrix-vector product $\boldsymbol{Tx}$ can be calculated with great efficiency and without explicit storage of the full representation of $\boldsymbol{T}$. While special methods have been devised to exploit similar characteristics of the non-relativistic propagation equations, it is sufficient to use a standard, general method for the solution of the time-dependent Dirac equation, such as the conjugate gradient method.[181]

In this case, it is always possible to construct the matrix $\boldsymbol{T}$ to be close to the unit matrix, simply by selecting δt to be sufficiently small. In this case, the solution of the equations represented by $\boldsymbol{Tx} = \boldsymbol{b}$ is said to be 'pre-conditioned', and the iterative algorithm that determines the vector $\boldsymbol{x}$ is rapidly convergent if a suitable starting guess can be found. A particularly good starting guess is

$$\boldsymbol{\Psi}(t+\delta t)\simeq[1-i\hat{H}(t+\delta t/2)\delta t]\boldsymbol{\Psi}(t) \tag{97}$$

which is just the explicit step, $\boldsymbol{\Psi}(t) \rightarrow \boldsymbol{\Psi}(t + \delta t)$, using the first-order approximation to the propagator. The implicit scheme is then used to refine the solution iteratively by a conjugate gradient search, in precisely the same way that similar discretization schemes are used to solve the time-dependent Schrödinger equation in the velocity gauge. In this scheme, we are not attempting to solve an, explicit, stiff set of coupled differential equations, but are, instead, employing an implicit scheme to maintain stability. There are no rapidly-varying oscillatory terms in the present case because we do not employ a spectral expansion.

5.3 Application: above threshold ionization

In the first application of a time-dependent description of wavefunction propagation, the photoionization spectrum is monitored. This gives a direct measure of the composition of the wavefunction that is generated through the driving influence of the time-dependent interaction with an intense field. If $\boldsymbol{\Psi}(\tau)$ represents the wavefunction at the completion of the pulse, then we may exploit the completeness of the complete set of solutions of the Dirac equation by writing it in the form

$$\boldsymbol{\Psi}(\tau)=\sum_k a_k\boldsymbol{\psi}_k(\boldsymbol{r})\exp(-iE_kt) \tag{98}$$

so that population of each level, p_k, is given by $p_k = |a_k|^2$, or

$$p_k = |\langle\boldsymbol{\psi}_k|\boldsymbol{\Psi}\rangle|^2. \tag{99}$$

From this point of view, only those $\boldsymbol{\psi}_k$ that correspond to positive-energy continuum states are of interest, since only these possess sufficient kinetic energy to propagate to the detector, which is assumed to be far distant from the residual ion. The components of this expansion involving the bound-states and the negative energy states remain localized at the position of the residual ion and evolve in time until no residual force is exerted on the ion, eventually forming a system at electrostatic equilibrium.

5.4 Application: high-harmonic generation

In classical electromagnetic theory, an accelerating charge radiates, and one may readily calculate the differential power radiated by an accelerating charge. The differential rate of power flow per unit solid angle is given by[182]

$$\frac{\mathrm{d}P(t)}{\mathrm{d}\Omega}=|\boldsymbol{A}(t)|^2 \tag{100}$$

where

$$\boldsymbol{A}(t)=\sqrt{\frac{c}{4\pi}}r\boldsymbol{E}(t) \tag{101}$$

where r is the observer-particle distance so that the differential energy passing through unit solid angle is

$$\frac{\mathrm{d}W}{\mathrm{d}\Omega}=\int_{-\infty}^{\infty}|\boldsymbol{A}(t)|^2\mathrm{d}t. \tag{102}$$

The frequency spectrum of the accelerating particle is given by the Fourier transform

$$\boldsymbol{A}(\omega) = \sqrt{\frac{1}{2\pi}}\int_{-\infty}^{\infty} \boldsymbol{A}(t)\exp(i\omega t)\mathrm{d}t. \tag{103}$$

By Parseval's theorem, we must also have

$$\frac{\mathrm{d}W}{\mathrm{d}\Omega} = \int_{-\infty}^{\infty} |\boldsymbol{A}(\omega)|^2 \mathrm{d}\omega. \tag{104}$$

The frequency representation of the differential power emitted into solid angle Ω is given by[183]

$$\frac{\mathrm{d}^2W}{\mathrm{d}\omega\mathrm{d}\Omega} = \frac{e^2}{4\pi^2 c}\left|\int_{-\infty}^{\infty}\mathrm{d}t\left\{\frac{\boldsymbol{n}\times[\boldsymbol{n}-\boldsymbol{\beta}]\times\dot{\boldsymbol{\beta}}}{(1-\boldsymbol{\beta}\cdot\boldsymbol{n})^2}\right\}\right. \times \exp[i\omega(t-\boldsymbol{n}\cdot\boldsymbol{r}_0(t)/c)]\Big|^2 \tag{105}$$

Here $\boldsymbol{\beta} = v/c$, $\boldsymbol{n} = (\boldsymbol{x}-\boldsymbol{r}_0)/r$, $\boldsymbol{x}$ is the observer position and $\boldsymbol{r}_0$ the particle trajectory. In the non-relativistic limit, $\beta \ll 1$. If we also assume that the amplitude of motion of the electron is much smaller than the distance to the observer, then we may take r to be a constant, and the particle acts essentially like a point source.

Under these circumstances, the differential energy emitted per unit frequency and per unit solid angle is given, to a good approximation, by

$$\frac{\mathrm{d}^2W}{\mathrm{d}\omega\mathrm{d}\Omega} = \frac{e^2}{2\pi c^3}|\boldsymbol{a}_\perp(\omega)|^2 \tag{106}$$

where we define $\boldsymbol{\alpha}_\perp(t) = c\dot{\boldsymbol{\beta}}_\perp(t)$ and $\boldsymbol{a}_\perp(\omega)$ is its Fourier transform.

If we start from the classical non-relativistic formula for the differential energy for a point particle, this may be transformed into a form suitable for calculation using quantum mechanical amplitudes by integrating over the electron density distribution. As a consequence,

$$\frac{\mathrm{d}^2\langle W\rangle}{\mathrm{d}\omega\mathrm{d}\Omega} = \frac{e^2}{2\pi c^3}|\langle\boldsymbol{a}\rangle_\perp(\omega)|^2 \tag{107}$$

where $\langle\cdot\rangle$ denotes an expectation value in the time dependent density, $\rho(\boldsymbol{x},t) = \boldsymbol{\psi}^*(\boldsymbol{x},t)\boldsymbol{\psi}(\boldsymbol{x},t)$.

According to Ehrenfest's theorem, we may evaluate the required expectation value by noting that

$$m\langle\boldsymbol{a}\rangle = \left\langle e\boldsymbol{E} + \frac{e}{c}\boldsymbol{v}\times\boldsymbol{B}\right\rangle \tag{108}$$

for an electron subjected to the Lorentz force from a particular configuration of external electric and magnetic fields.

Consider an electron subjected to an intense classical time-dependent electric field, such as that occurs during the interaction of an atom with a strong laser field. The interaction causes the electron to accelerate, due to the dipolar interaction, which is of the form $e\boldsymbol{r}\cdot\boldsymbol{E}$.

Since the electron is forced out of equilibrium by the external radiation field, it becomes subject to the residual Coulomb field of the atomic nucleus. It experiences a time-dependent dipole acceleration of the form

$$\boldsymbol{a}(t) = \frac{Ze}{4\pi\varepsilon_0 m}\int \boldsymbol{\psi}^*(\boldsymbol{x},t)\frac{1}{r^2}\boldsymbol{\psi}(\boldsymbol{x},t)d^3x. \tag{109}$$

If the Coulomb field is supplemented by an additional model mean-field, such as a Kohn–Sham potential, one must also include the spatial derivative of this potential in the calculation of the net acceleration to which the electron is subjected. A time-dependent approach to this problem appears in the next section. Recollisions of the accelerated electron packet with this field cause it to radiate whenever its density offers a significant overlap with the region occupied by the ground-state. In all other regions the electron, which is essentially free, absorbs multiple photons from the laser field, and this energy is liberated during the Coulomb acceleration process.

This is the physical origin of high-harmonic generation and the formalism is equally valid whether $\boldsymbol{\psi}(\boldsymbol{x},t)$ represents a Schrödinger wavefunction or a Dirac spinor. A driving laser whose frequency is in the optical or infra-red region of the spectrum may be used to generate VUV or XUV light by the non-linear response of the atom to the external radiation force, and the sudden acceleration caused when the distorted wavepacket re-encounters the Coulomb field.

The frequency spectrum and angular distribution from a high-harmonic source is obtained by calculating the Fourier transform of $\boldsymbol{a}_\perp(t)$, yielding $\boldsymbol{a}_\perp(\omega)$, which is then substituted into eqn (107) to obtain the energy produced per unit solid angle per unit frequency.

The significance of eqn (73,74) is now apparent. If we may model the interaction of the electron with the field as a classical time-dependent electric dipole interaction, the motion of the electron, and its time-dependent acceleration, is essentially one-dimensional. An electron that is initially in an atomic bound-state will be accelerated in a direction transverse to the direction of propagation of the incident field. Consequently, there is a high probability that the electron will recollide with the residual ion, causing the acceleration of the charge that leads to high-harmonic radiation. If the incident field strength exceeds approximately 1×10^{15} W cm^2 at optical frequencies, however, non-dipole effects give rise to an effective magnetic interaction that causes the excited electronic wavepacket to drift in the direction of propagation of the illumination; the motion is now two-dimensional. The probability of recollision of the wavepacket with the residual ion is reduced and the emission of high-harmonic radiation is suppressed, because there is negligible acceleration of the charge, other than that due to the driving field, in any direction that is transverse to a far-field observer.

6 DKS real-time propagation using G-spinors

Time-dependent density functional theory (TDDFT) has become a widely-used method to compute molecular dynamics properties such as excited-state energies.[184,185] Usually the approach is based on the linear response theory with frequency, rather than time, as the independent variable. In this case, a time-independent eigenvalue equation may be derived[186,187] to obtain the excitation spectrum. This linear system has solution

for certain discrete eigenvalues that correspond to the excitation energies. So in the linear response regime for the excitation energies and optical spectra, the theoretical modelling basically proceeds in two steps: initially, the self-consistent-field (SCF) solutions of the Kohn–Sham (KS) equation are sought to obtain ground state properties and a first approximation for the excitation energies as transitions between occupied and virtual KS orbitals. In a second step the energies and related optical oscillator strengths are corrected for the so-called Coulomb-exchange–correlation kernel.

This approach has been extended pragmatically to the four-component DKS formalism by the group of Liu.[41] It permitted for the first time to account for spin–orbit coupling within the time-dependent DFT for excitation energies. The method has been further extended by using a noncollinear form for the exchange–correlation kernel.[42] Bast *et al.*[43] have recently reported an implementation of adiabatic TDDFT based on the DKS method that includes noncollinear spin magnetization, hybrid GGA functionals, and full derivatives of the functionals for the exchange–correlation kernel. Both of these implementations are *de facto* proofs of the potential offered by a full four-component framework for the investigation of excited-state chemistry of molecules containing heavy atoms, including spin–orbit effects.

An approach based on first-order response however is insufficient to study atoms or molecules in intense laser pulses. This subject has received considerable attention in recent times, in particular following the availability of femto- and atto-second pulses, which has made possible to probe and control the behavior of molecules in strong fields and promises great technological advances. We have already reviewed the relativistic one-electron theory of strong-field laser-matter interactions, which we now extend to a time-dependent density-functional treatment of many-electron systems. To describe electronic systems in these regimes, a real-time propagation approach is required, and one seeks to solve the Kohn–Sham equation directly in the real-time domain. Several non-relativistic implementations have been presented (see for instance ref. 188–190 and references therein) after the pioneristic work of Yabana and Bertsch.[191] Most of the implementations are based on a real-space grid methodology, but some recent effective implementations using Gaussian basis functions have also appeared.[188,189] The real-time propagation approach has been used in several contexts with increasing success to study, for example, linear[192,193] and non-linear properties,[194,195] core excitations,[196] conductance analysis[189] high-harmonic generation,[197,198] photoinduced electric currents in molecules.[199] For a recent review see, *e.g.*, ref. 198.

There are many advantages associated with the real-time formulation of TDDFT. From the computational point of view, the method presents reduced scaling properties. Only occupied states are used in the calculation, in contrast to the perturbative approach in which one has to construct and diagonalize a super-matrix involving all occupied and unoccupied orbitals. The implementation is relatively simple, since one can make use of essentially the same operations already used in the computation of ground state properties. The non-linear effects are automatically accounted for and effects due to the specific profile of the external field can be easily included. The calculations of non-linear polarizabilities become more transparent and the explicit kernel derivatives appearing in the linear response approach are avoided. The only added computational effort of real-time propagation approaches is the evaluation of the time evolution operator, which involves the repeated calculation of the Hamiltonian at each time step. The method can be easily extended to the relativistic four-component DKS domain. Its extension is particularly desirable because it would represent an important step forward towards the understanding of relativistic and spin-dynamics effects in optical properties, high-harmonic generation, and molecular electronic transport properties.

A simple and direct generalization of the real-time Kohn–Sham equation can be easily envisaged. Starting with the DKS formulation, one can obtain an effective one particle time-dependent Dirac equation (TDDKS) for the DKS orbitals

$$\boldsymbol{H}_{\mathrm{DKS}}\boldsymbol{\Psi}_i(\mathrm{r},t) = i\frac{\mathrm{d}\boldsymbol{\Psi}_i(\boldsymbol{r},t)}{\mathrm{d}t} \qquad (110)$$

The Hamiltonian $\boldsymbol{H}_{\mathrm{DKS}}$ depends on the four-current density. If we restrict ourselves to a longitudinal potential and use the adiabatic approximation,[200] $\boldsymbol{H}_{\mathrm{DKS}}$ takes on the simplified form:

$$\boldsymbol{H}_{\mathrm{DKS}} = c\boldsymbol{\alpha}\cdot\boldsymbol{p} + \boldsymbol{\beta}c^2 + v^{(\mathrm{l})}[\rho(t)] + v_{\mathrm{ext}}(t) \qquad (111)$$

The adiabatic approximation assumes that the Hamiltonian depends only on the density at time t. $v_{\mathrm{ext}}(t)$ is an external potential including any time-dependent field and $v^{(\mathrm{l})}[\rho(t)]$ is the longitudinal potential comprising the Coulomb-exchange–correlation potential and the potential due to the nuclei.

The TDDKS equation may be formally integrated to give

$$\boldsymbol{\Psi}_i(t+\Delta t) = \boldsymbol{U}(t+\Delta t,t)\boldsymbol{\Psi}_i(t) \qquad (112)$$

where the time evolution operator $\boldsymbol{U}(t+\Delta t,t)$ is given by

$$\boldsymbol{U}(t+\Delta t,t) = T\exp\{-i\textstyle\int_t^{t+\Delta t}\boldsymbol{H}_{\mathrm{DKS}}(\tau)\mathrm{d}\tau\} \qquad (113)$$

and T is the time-ordering operator, ensuring that operators associated with later times always appear to the left of those associated with earlier times. While the external electric field may be explicitly dependent on time, $v^{\mathrm{L}}[\rho(t)]$ has an implicit time dependence through the density $\rho(t)$. This implicit time dependence represents the core challenging aspect of these equations.

In terms of the one-particle density matrix the TDDKS equation is written as

$$i\frac{\mathrm{d}\boldsymbol{D}(t)}{\mathrm{d}t} = [\boldsymbol{H}_{\mathrm{DKS}}(t),\boldsymbol{D}(t)] \qquad (114)$$

The propagation of the density matrix is then obtained as

$$\boldsymbol{D}(t+\Delta t) = \boldsymbol{U}(t+\Delta t,t)\boldsymbol{D}(t)\boldsymbol{U}^{\dagger}(t+\Delta t,t) \qquad (115)$$

One may decide to propagate in time either the DKS spinors, eqn (112), or directly the density matrix, eqn (115). Besides the respective associated linear algebra operations, the key step is in any case the evaluation of the evolution operator eqn (113). One can here use the straightforward extension of the propagation algorithms proposed in the time-dependent nonrelativistic DFT framework (see for instance ref. 180 and 188 and references therein). The computationally demanding operation is the evaluation of the Hamiltonian matrix and,

therefore, the calculation is primarily accelerated by adopting computational strategies that minimize the number of Hamiltonian evaluations required and/or that make such evaluation particularly efficient. This latter aspect makes our parallel density-fitting DKS implementation particularly well suited.

In a simulation, the total propagation interval is typically divided into many small steps Δt and an approximation to eqn (113) computed at each time step. Non-relativistic implementations based on the use of Gaussian basis sets seem to suggest that the second order Magnus expansion in combination with a predictor–corrector scheme can ensure a rapidly convergent approximation. Accordingly, the time evolution operator from t to $t + \Delta t$ is approximated as

$$\boldsymbol{U}(t+\Delta t,t)=\exp\{-i\boldsymbol{H}_{\mathrm{DKS}}(t+\Delta t/2)\Delta t/2\}+O(\Delta t^3) \quad (116)$$

For sufficiently small Δt the second order Magnus expansion can provide accurate results. However, here one still needs to evaluate $\boldsymbol{H}_{\mathrm{DKS}}(t + \Delta t/2)$, which depends on the yet unknown density matrix at time $t + \Delta t/2$. This problem is solved by a predictor–corrector step, in which the DKS matrices $\boldsymbol{H}_{\mathrm{DKS}}(t - \Delta t/2)$ and $\boldsymbol{H}_{\mathrm{DKS}}(t - 3\Delta t/2)$ are used to extrapolate an estimate to $\boldsymbol{H}_{\mathrm{DKS}}(t + \Delta t/4)$. This is then used to compute $\boldsymbol{U}(t + \Delta t/2)$ from eqn (116) and then propagate $\boldsymbol{D}$ from time t to time $t + \Delta t/2$ according to eqn (115), with which the required $\boldsymbol{H}_{\mathrm{DKS}}(t + \Delta t/2)$ can be built. The algorithm has been well described in ref. 189 and applied with success.[188]

The key quantity in a real time TDDFT simulation is the total polarization $\boldsymbol{P}(t)$ defined as

$$\boldsymbol{P}(t) = \int \rho(t,\boldsymbol{r})\boldsymbol{r}\mathrm{d}\boldsymbol{r} \quad (117)$$

The $\boldsymbol{P}(t)$ thus defines the polarization response to all orders and it is easily computed by the electronic density at the time t, $\rho(t,\boldsymbol{r})$. From this simple quantity one can easily compute linear and non-linear properties.

In the linear response regime each component of the polarization in frequency space assuming an external field E_q in the direction q is given by

$$P_p(\omega) = \alpha_{pq}(\omega)E_q(\omega) \quad (118)$$

The absorption cross section $\sigma(\omega)$ is related to the imaginary part of the frequency dependent linear polarizability by

$$\sigma(\omega) \approx \omega\ \mathrm{Im}\frac{\mathrm{Tr}\ \boldsymbol{\alpha}(\omega)}{3} \quad (119)$$

High-harmonic generation occurs *via* photoemission by the molecular system in a strong field. It can be conveniently computed[201] as the Fourier transform of the polarization acceleration as

$$\sigma_{\mathrm{H}}(\omega) \approx \left|\int \frac{\mathrm{d}^2\boldsymbol{P}(t)}{\mathrm{d}t^2}\mathrm{e}^{-i\omega t}\mathrm{d}t\right|^2 \quad (120)$$

which is equivalent to the expression for the atomic high-harmonic spectrum derived in eqn (106).

As we said above, usually the computation cost in non-relativistic implementations of real time TDDFT based on Gaussian basis sets is dominated by the Kohn–Sham matrix construction at each time step, the rest of the processing time being spent in simple linear algebra operations. Therefore, an efficient and successful implementation of the TD-DKS method has as prerequisite the highly efficient evaluation of the DKS matrix. As we have underlined in this work the efficiency achieved using our parallel implementation of the density fitting approach to the construction of the DKS matrix is in this respect particularly promising.

7 Relativistic exchange–correlation functionals: a brief outlook

The genuine relativistic exchange–correlation functionals should depend on the relativistic four-current.[15] But the research activity on these functionals is still at an early stage and mostly limited to the non-relativistic framework. We will briefly comment on the perspectives in this field at the end of this section.

Exchange–correlation functionals explicitly designed for relativistic calculations are still essentially unavailable and therefore, pragmatically, it is common practice to use non-relativistic functionals, even in four-component molecular DKS codes. The use of non-relativistic density-dependent functionals can be justified for closed-shell atoms and molecules. In these cases the spatial component of the four-current vanishes ($\boldsymbol{j} = 0$) and so the Hartree potential is only longitudinal, as it is in non-relativistic DFT. One may thus expect that the existing non-relativistic exchange energy functionals may serve as reasonable first approximations to the relativistic longitudinal exchange energy functionals. Moreover, it seems also reasonable to assume that the use of a non-relativistic form for the correlation functional should recover most of the correlation energy, as this comes mainly from the valence electrons. Of course, it must in general be expected that, in the relativistic context, the performance of a given non-relativistic exchange–correlation functional is at best comparable to that exhibited in non-relativistic calculations. The situation is further more involved in case one wishes to compute the electronic structure of open-shell molecular systems.[98] In non-relativistic DFT, in order to describe accurately open-shell systems, one resorts to spin DFT, in which spin-polarized densities are tracked independently and the exchange–correlation functionals are functionals of the polarized density ("spin up" and "spin down"). For example, non-relativistic density functionals falling within the GGA class[202] are written in the form

$$E^{\mathrm{xc}} = \int f(\rho_\alpha,\rho_\beta,\gamma_{\alpha\alpha},\gamma_{\alpha\beta},\gamma_{\beta\beta})\mathrm{d}\boldsymbol{r} \quad (121)$$

where

$$\rho_\xi = \sum_i |\psi_{i,\xi}|^2 \quad (122)$$

$$\gamma_{\xi\xi'} = \nabla\rho_\xi\cdot\nabla\rho_{\xi'} \quad (123)$$

where $\xi = \alpha,\beta$ and $\psi_{i,\alpha}$, $\psi_{i,\beta}$ are the one-electron solutions of the non-relativistic Kohn–Sham equation with spin α and β, respectively.

A technical and conceptual difficulty arises for the definition of the spin density in a relativistic framework where spin is no longer a good quantum number. The formal connection between the spin density and the current is given by the Gordon decomposition of the three-current. For a stationary state it reads:[203]

$$\boldsymbol{j} = \boldsymbol{I} + \nabla\times\boldsymbol{S} \quad (124)$$

where $\boldsymbol{I}$ is the orbital current density and is related to the orbital magnetization. $\boldsymbol{S}$ is the vector of elements $S_\tau = \frac{1}{2}\sum_i \boldsymbol{\Psi}_i^\dagger \beta \boldsymbol{\Sigma}_\tau \boldsymbol{\Psi}_i$, where the sum runs over the electronic spinors, $\tau = x,y,z$, and $\boldsymbol{\Sigma}_x,\boldsymbol{\Sigma}_y,\boldsymbol{\Sigma}_z$ are the components of the spin density. Only in the approximation in which the full magnetization density is due to the spin component (this means neglecting completely the contribution of the orbital current density $\boldsymbol{I}$ in eqn (124)) can the exchange–correlation functional be expressed as a functional of charge density and spin magnetization (s). In non-relativistic theory, because the spin and spatial degrees of freedom are completely decoupled, one can choose freely a quantization axis for the spin angular momentum. Thus, a simple adaptation of the non-relativistic spin density to the four-component relativistic framework would be, for instance, to use the 4×4 spin operator $\boldsymbol{\Sigma}_\tau$ and define spin density as

$$s = \sum_i \Psi_i^\dagger \Sigma_z \Psi_i. \qquad (125)$$

This definition is referred in the literature as the "collinear" approach.[98] In this case the direction of magnetization is fixed. The collinear approach breaks the rotational invariance of the energy, which is of course a very undesirable feature when performing molecular DFT calculations. This has been shown by van Wüllen.[204] Different approaches have been investigated by several researchers (see for instance ref. 89, 90 and 98). A solution is to invoke the so-called non-collinear approach, where one considers a more general definition of the spin density and the corresponding spin polarization, by using for s the norm of the spin magnetization vector, so that one can substitute in eqn (121) $\rho_\alpha = \frac{1}{2}(\rho + s)$ and $\rho_\beta = \frac{1}{2}(\rho - s)$ with $s = \rho_\alpha - \rho_\beta \geq 0$ and employ standard non-relativistic functionals. It has to be noted that spin magnetization is only a device for encoding information about the four-current density. It is clear that in a fully fledged relativistic DFT, spin-magnetization will have to be replaced by the four-current, as soon as appropriate functionals become available.

Before going on describing the typical performance of DKS calculations using non-relativistic exchange–correlation functionals it is useful to underline that the same distinction between collinear and non-collinear approaches and the same problems associated with the collinear approximation apply to the kernel functionals in TDDFT and their derivatives (see for example ref. 42, 43 and 205).

The most widely used exchange–correlation functionals in DKS calculations are the simple explicitly density-dependent functionals that appear in local density approximations (LDA) and in GGA gradient corrected approximations. The implementation of these functionals is relatively simple because they depend only on the charge density (LDA) or, in addition, its derivatives (GGA). In this last case the functional is not strictly local, but includes information on the deviations from homogeneity provided by the density gradient.

With the use of non-relativistic exchange–correlation functionals, relativistic corrections to the exchange–correlation energy arise only from the use of a relativistic density. The contribution that may result from the modification of the functional form due to relativity[61] has been investigated[70,206] some time ago in the case of LDA and GGA functionals. These corrections take the form of a density-dependent factor multiplying the non-relativistic functional. Thus, the essential non-relativistic functional form is retained and detailed relativistic effects are not included. This approach is simple to implement and is directly relevant only in the high-density regime, corresponding to the innermost (core) orbitals. Varga *et al.*[61] made a thorough examination of these relativistic corrections to some well-established exchange–correlation energy functionals. They found that such corrections to the exchange–correlation functionals give no significant contribution to the binding energies or spectroscopic constants of a number of diatomic homo-nuclear molecules. The performance of these corrections for the calculation of properties that depends on the electronic density close to the nuclei has not been investigated in detail.

Systematic studies aimed at analyzing the performance of different functionals in DKS calculations are also scarce. They would be highly desirable in order to assess the level of accuracy one may expect when using typical non-relativistic functionals in DKS calculations. An example of this kind of studies is given by Fossgaard *et al.*,[115] who have investigated systematically, and with an extended basis set, the ground state spectroscopic properties of a set of 14 molecules: the hydrogen halides HX, the dihalogens X_2, as well as the inter-halogens XY (X, Y = F, Cl, Br, and I) using several non-relativistic exchange–correlation functionals including LDA, GGA and the hybrid functional B3LYP. A comparison between DKS calculations and accurate CCSD(T) calculation using the same basis set indicates that non-relativistic functionals perform well in the four-component framework. The most striking result was in fact the overall good performance of the simple LDA functional, which reproduced bond lengths, harmonic frequencies and dipole moments with average relative errors of 0.5%, 0.4%, −0.7%, respectively. GGA functionals like BLYP were found to systematically overestimate bond length and underestimate harmonic frequencies. The performance improved significantly upon including a part of the exact exchange with the B3LYP functional. A quite different picture emerges, however, in the study of molecular systems containing heavy atoms, such as MAu with M an alkali metal. In this case the LDA approximation yields too strong bonds (by 0.32 eV for CsAu) and predicts a too short bond length (by 0.15 Å for CsAu), as is typical of this functional in the non-relativistic context. As to the effects of the inclusion of the exact exchange, it may be mentioned that the BLYP and B3LYP functionals have both been found to give results in consistently good agreement with four-component CCSD(T) computations (see ref. 207 and 208 and references therein). Again for CsAu, the error in the bond length and dissociation energy is less than 0.05 Å and 0.12 eV, respectively. Less satisfactory results, however, have been obtained for the dipole moment, underestimated by about 10% in these systems.

Recently, Thierfelder *et al.*[209] investigated closed-shell mono-hydrides of super-heavy elements, showing that the DKS approach in combination with standard exchange–correlation functionals performs reasonably well, in fair agreement with DC-CCSD(T) calculations. The quality of the results was found to be largely independent of the exchange–correlation potential used. The DKS calculations overestimate slightly the

bond length (on average by only 0.02, 0.03 and 0.04 Å, using the LDA, B3LYP and PBE functionals, respectively), while they slightly underestimate the harmonic forces by 8, 6 and 22 N m^{-1}.

The applications of the spin density approach in either the collinear or non-collinear scheme for the prediction of molecular properties are also somewhat scarce.[89,90,92] The results found were surprisingly close to the best experimental findings (see for example),[92] although a study of basis-set convergence was not made.

An all-electron DKS method is clearly appealing because one can in principle treat consistently on the same footing both the valence and core electronic structure with the proper inclusion of relativistic effects. These are crucial for a proper description of core properties. An example of the difficulties that may arise using standard functionals in the computation of core properties is provided by the EFG, one of the core-electron properties most systematically investigated at the DKS level. The accurate computation of the EFG at the nuclei can be used, combined with experimental observations, to give an estimate of the nuclear quadrupole moment (NQM) (see for instance ref. 210 and references therein). In the case of heavy atoms reliable predictions are really challenging. Schwerdtfeger *et al.*[211] showed that due to the conservation of the number of particles, a change in the valence part of the electron density can lead to changes in the core part of the density. Thus, errors in valence electronic properties like the dipole moment may affect the evaluation of core properties like the EFG. Many investigations have shown that common exchange–correlation functionals (LDA, GGA including hybrid functionals) produce inaccurate EFG values at the nuclei of transition metals and heavy atoms in molecular calculations. An example of this is given by the case of ^{137}Au.[210] Belpassi *et al.*[212] used an indirect approach where the NQM is determined from the changes in the EFG along a series of molecules. They showed that, at least in a series of chemically strictly related molecules (AuF, XeAuF, KrAuF, ArAuF, (CO)AuF), EFG variations can be computed quite accurately leading to much more reliable estimates of the NQM of ^{137}Au, in close agreement with DC-CCSD(T) results. This suggests the presence of a systematic error that is not directly related to the relativistic DFT framework, but rather to deficiencies in the description of the exchange–correlation in the valence region. It was indeed argued that a systematic error in the computation of the EFG originates from an incorrect description of the charge distribution in the valence region afforded by standard functionals.[213] A basic electric property like the dipole moment is underestimated in some cases by more than 0.5 D for the group-11 halides if one uses standard GGA functionals. By contrast, the use of an exchange functional (CAM-B3LYP) possessing the correct long-range behavior, and which accurately reproduces the dipole moment of AuF, resulted in reasonably accurate values of the NQM of ^{63}Cu and ^{197}Au.[35] This example clearly suggests that the potentiality of an all-electron approach for the determination of core-electron properties can be fully realized only if more accurate exchange–correlation functionals are designed. This appears to be a key aspect in order to extend further the applicability and accuracy of the DKS method.

Many of the shortcomings of the use of LDA or GGA functionals in the DKS framework are the same found in the non-relativistic context. For an extensive review see for instance ref. 13. Such is, for example, the well known self-interaction error, which also affects functionals incorporating a part of the exact exchange and is due to the incomplete cancellation of the spurious repulsion of an electron with itself included in the Hartree potential. A consequence of this deficiency is the incorrect asymptotic exponential decay of the corresponding exchange–correlation potentials for finite systems and has important negative consequences for chemical applications (see ref. 214).

The development of new, improved functionals is an ongoing effort. We envisage three main areas of intervention specifically oriented towards the DKS method and the goal of an accurate description of systems containing heavy atoms.

(1) A promising endeavor is to build on the long experience in the development of the empirical and semi-empirical exchange–correlation functionals in the non-relativistic context. Many exchange–correlation functionals depend on a set of parameters that are obtained by the best fit on a set of atoms or molecules in order to obtain accurate results for a given property. Most often optimization has been restricted to light-atom systems. Research should be devoted to improve and eventually optimize standard functionals in the DKS framework and including in the data set molecules containing heavy atoms.

(2) The use of orbital dependent functionals, in particular for the full exact exchange, arguably represents the most promising development in DFT to overcome the shortcomings of GGA and hybrid methods. A treatment based on the orbital-dependent exchange energy is appealing because, besides providing an exact evaluation of this energy term, it eliminates the self-interaction error and displays a potential having the correct asymptotic behavior $(-1/r)$.

The exact DKS exchange energy in terms of the molecular spinors (see for instance page 553 of ref. 3) is given by

$$E_x = -\frac{1}{2}\sum_{i,j}\int \frac{\Psi_i^\dagger(\boldsymbol{r})\Psi_j(\boldsymbol{r})\Psi_j^\dagger(\boldsymbol{r}')\Psi_i(\boldsymbol{r}')}{|\boldsymbol{r}-\boldsymbol{r}'|}\mathrm{d}\boldsymbol{r}\mathrm{d}\boldsymbol{r}' + \frac{1}{2c^2}\sum_{i,j}\int \frac{(\Psi_i^\dagger(\boldsymbol{r})\boldsymbol{\alpha}\Psi_j(\boldsymbol{r}))\cdot(\Psi_j^\dagger(\boldsymbol{r}')\boldsymbol{\alpha}\Psi_i(\boldsymbol{r}'))}{|\boldsymbol{r}-\boldsymbol{r}'|}\mathrm{d}\boldsymbol{r}\mathrm{d}\boldsymbol{r}' \quad (126)$$

where the sum extends over the occupied positive-energy states. $E_x[j^\mu]$ represents an implicit functional of the four-current: the DKS spinors are unique functionals of j^μ by virtue of the relativistic generalization of the Hohenberg–Kohn theorem.

Given an explicit spinor dependent functional, the main task is to derive a relation that allows the calculations of the corresponding potential. An appropriate method, called the optimized potential method (OPM), was proposed by Talman and Shadwick[215] and a fully relativistic four-current version (ROPM) has been presented by Engel *et al.*[216] The basic idea is that relativistic DKS spinors are unique functionals of j^μ and therefore the functional derivatives of E_{xc} with respect to j^μ can be expressed, for the evaluation of the local exchange–correlation

potential v_{xc}^{μ}, in terms of appropriate functional derivatives with respect to the spinors Ψ_k.

This potential is the solution of an integral equation

$$\int \chi^{\mu\nu}(\boldsymbol{r},\boldsymbol{r}')v_{xc,\nu}(\boldsymbol{r}')\mathrm{d}\boldsymbol{r}' = \lambda_{xc}^{\mu}(\boldsymbol{r}) \quad (127)$$

where, in the non-virtual pair (NVP) approximation that consider only positive energy solutions, $\chi^{\mu\nu}(\boldsymbol{r},\boldsymbol{r}')$ is defined in terms of the static DKS response function $G_k(\boldsymbol{r},\boldsymbol{r}')$

$$\chi^{\mu\nu}(\boldsymbol{r},\boldsymbol{r}') = -\sum_k \Psi_k^{\dagger}(\boldsymbol{r})\alpha^{\mu}G_k(\boldsymbol{r},\boldsymbol{r}')\alpha^{\nu}\Psi_k(\boldsymbol{r}') + c.c. \quad (128)$$

$$G_k(\boldsymbol{r},\boldsymbol{r}') = \sum_{l\neq k} \frac{\Psi_l(\boldsymbol{r})\Psi_l(\boldsymbol{r}')}{\varepsilon_l - \varepsilon_k} \quad (129)$$

where k runs over only the positive-energy states.

The inhomogeneous term $\lambda_{xc}^{\mu}(\boldsymbol{r})$ is given by

$$\lambda_{xc}^{\mu}(\boldsymbol{r}) = -\sum_k \int [\Psi_k^{\dagger}(\boldsymbol{r})\alpha^{\mu}G_k(\boldsymbol{r},\boldsymbol{r}')\frac{\delta E_{xc}}{\delta\Psi_k^{\dagger}(\boldsymbol{r}')} + c.c.]\mathrm{d}\boldsymbol{r}' \quad (130)$$

The numerical evaluation of eqn (127) is complicated. It is an integral equation involving the full set of occupied and unoccupied DKS orbitals and eigenvalues, which in principle has to be solved self-consistently with the DKS equation. Most of the research effort, both relativistic and non-relativistic, goes into finding simplifications, which usually consist in adopting an approximate expression of Green's function $G_k(\boldsymbol{r},\boldsymbol{r}')$. One of the most common is the Krieger–Li–Iafrate (KLI) approximation,[217] which has been successfully extended to the relativistic domain.[216] In cases where only the longitudinal component of the exchange–correlation potential was considered, this approach has led to total energies and spinor eigenvalues in close agreement with the corresponding true OPM solution. Recently the OPM approach has been introduced into relativistic spin-density functional theory by Engel *et al.*,[218,219] who reported satisfactory results for a number of free atoms and discussed potential extensions of the method for the solid state.

In the non-relativistic context a similar optimized effective potential approach, the localized Hartree–Fock potential method, has been proposed[220] which defines a non-self-consistent procedure to obtain an approximation to the exact orbital-dependent exchange. This has been particularly successful for DFT exact-exchange studies of molecular systems employing Gaussian basis functions. The approach is notable for its high numerical stability and computational efficiency, being in addition particularly suitable for use with density fitting techniques.[221] Its relativistic extension to the DKS framework appears therefore particularly desirable and suitable for implementation within our DKS approach using G-spinor basis sets and density fitting.

(3) The development of current-dependent functionals is a relatively new field and, to date, no explicit relativistic four-current functional has yet been proposed. The non-relativistic current-density functional theory (CDFT) was formulated by Vignale and Rasolt in the late eighties.[222,223] More recently Bencheikh[224] has further extended spin-CDFT to incorporate the spin–orbit interaction. Typically, the attempts made to find a current-dependent functional have started from the Gordon decomposition of the three-current and proceeded to define functionals of the charge density, spin density and paramagnetic current (see for instance ref. 225 and references therein). There doesn't seem to have been any attempt to define directly functionals of the relativistic four-current.[226] This is thus a completely unexplored and potentially very promising field.

8 Conclusions and perspectives

All-electron four-component relativistic DFT calculations, even for very large heavy-atom systems and with extended basis sets, are well on their way to become a routine approach, not much differently than the standard non-relativistic or quasi-relativistic DFT methods. As reviewed in this paper, this very rapid development and extension of applicability range have been achieved through the concomitant efforts of a number of research groups. In the case of our own code, the key ingredients have been very efficient G-spinor integral evaluation algorithms, density fitting techniques and full data-distributed parallelism, overcoming the memory bottleneck. This opens the way to large-scale, accurate applications in hot areas such as cluster science or the chemistry of super-heavy elements but it will also stimulate related new research in advanced sectors such as the study of the interaction of molecules with strong fields through time-dependent approaches, and the design of even more accurate, current-dependent density functionals. We have illustrated and discussed here some realistic lines of development in these areas, concerning for example above-threshold ionization and high-harmonic generation, which we expect to be at the focus of considerable attention in the near future.

Acknowledgements

This work has been supported by the MIUR PRIN grant no. 2008KJX4SN_003. The latest computational developments and applications have been carried out under an Extreme Computing Initiative grant of the Distributed European Infrastructure for Supercomputing Applications (DEISA) and project HP10BO0PYX (AuCat) of the Italian SuperComputer Resource Allocation (ISCRA-CINECA).

References

1 P. Pyykkö and J. P. Desclaux, *Acc. Chem. Res.*, 1979, **12**, 276–281.
2 I. P. Grant, *Relativistic Quantum Theory of Atoms and Molecules: Theory and Computation*, Springer Science + Business Media, LLC, New York, NY, 2007.
3 *Relativistic Electronic Structure Theory. Part 1. Fundamentals*, ed. P. Schwerdtfeger, Elsevier, Amsterdam, 1st edn, 2002.
4 *Relativistic electronic structure theory. Part 2. Applications*, ed. P. Schwerdtfeger, Elsevier, Amsterdam, 1st edn, 2004.
5 M. Reiher and A. Wolf, *Relativistic Quantum Chemistry. The Fundamental Theory of Molecular Science*, Wiley-VCH, Weinheim, 2009.
6 C. Wüllen, in *Relativistic Methods for Chemists*, ed. M. Barysz and Y. Ishikawa, Springer Netherlands, 2010, vol. 10, pp. 191–214.
7 K. G. Dyall and K. Faegri Jr., *Introduction to Relativistic Quantum Chemistry*, Oxford University Press, Oxford, 2007.
8 U. Kaldor and S. Wilson, *Theoretical Chemistry and Physics of Heavy and Superheavy Elements*, Kluwer, Dordrecht, 2003.
9 *Recent Advances in Relativistic Molecular Theory*, ed. K. Hirao and Y. Ishikawa, World Scientific, Singapore, 2004, pp. 107–136.

10 P. Pyykkö, K. G. Dyall, A. G. Császár, G. Tarczay, O. L. Polyansky and J. Tennyson, *Phys. Rev. A: At., Mol., Opt. Phys.*, 2001, **63**, 024502.
11 G. Tarczay, A. G. Csaszar, W. Klopper and H. M. Quiney, *Mol. Phys.*, 2001, **99**, 1769.
12 B. Swirles, *Proc. R. Soc. London, Ser. A*, 1935, **152**, 625.
13 S. Kümmel and L. Kronik, *Rev. Mod. Phys.*, 2008, **80**, 3–60.
14 F. Mandl and G. Shaw, *Quantum Field Theory*, John Wiley and Sons, Chichester, 1984.
15 A. K. Rajagopal and J. Callaway, *Phys. Rev. B: Solid State*, 1973, **7**, 1912.
16 A. K. Rajagopal, *J. Phys. C: Solid State Phys.*, 1978, **11**, L943.
17 M. P. Das, M. V. Ramana and A. K. Rajagopal, *Phys. Rev. A: At., Mol., Opt. Phys.*, 1980, **22**, 9.
18 A. H. Macdonald and S. H. Vosko, *J. Phys. C: Solid State Phys.*, 1979, **12**, 2977.
19 E. Engel, S. Keller, A. F. Bonetti, H. Müller and R. M. Dreizler, *Phys. Rev. A: At., Mol., Opt. Phys.*, 1995, **52**, 2750–2764.
20 E. Engel and R. M. Dreizler, in *Topics in Current Chemistry*, ed. R. F. Nalewajski, Springer, 1996, vol. 181, p. 1.
21 W. Liu, G. Hong, D. Dai, L. Li and M. Dolg, *Theor. Chem. Acc.*, 1997, **96**, 75–83.
22 S. Varga, B. Fricke, H. Nakamatsu, T. Mukoyama, J. Anton, D. Geschke, A. Heitmann, E. Engel and T. Bastug, *J. Chem. Phys.*, 2000, **112**, 3499–3506.
23 T. Saue and T. Helgaker, *J. Comput. Chem.*, 2002, **23**, 814–823.
24 S. Komorovsky, M. Repisky, O. L. Malkina, V. G. Malkin, I. M. Ondik and M. Kaupp, *J. Chem. Phys.*, 2008, **128**, 104101.
25 T. Yanai, H. Iikura, T. Nakajima, Y. Ishikawa and K. Hirao, *J. Chem. Phys.*, 2001, **115**, 8267–8273.
26 H. M. Quiney and P. Belanzoni, *J. Chem. Phys.*, 2002, **117**, 5550–5563.
27 H. M. Quiney, H. Skaane and I. P. Grant, *J. Phys. B: At., Mol. Opt. Phys.*, 1997, **30**, L829.
28 H. M. Quiney, H. Skaane and I. P. Grant, in *Adv. Quantum Chem.*, ed. P.-O. Löwdin, Academic Press, 1998, vol. 32, pp. 1–49.
29 L. Belpassi, L. Storchi, F. Tarantelli, A. Sgamellotti and H. M. Quiney, *Future Gener. Comput. Syst.*, 2004, **20**, 739–747.
30 L. Belpassi, F. Tarantelli, A. Sgamellotti and H. M. Quiney, *J. Chem. Phys.*, 2005, **122**, 184109.
31 M. Patzschke and P. Pyykko, *Chem. Commun.*, 2004, 1982–1983.
32 M. Quack and J. Stohner, *Chimia*, 2005, **59**, 530–538.
33 P. Schwerdtfeger, T. Saue, J. N. P. van Stralen and L. Visscher, *Phys. Rev. A: At., Mol., Opt. Phys.*, 2005, **71**, 012103.
34 V. Weijo, R. Bast, P. Manninen, T. Saue and J. Vaara, *J. Chem. Phys.*, 2007, **126**, 074107.
35 C. Thierfelder, P. Schwerdtfeger and T. Saue, *Phys. Rev. A: At., Mol., Opt. Phys.*, 2007, **76**, 034502.
36 P. Salek, T. Helgaker and T. Saue, *Chem. Phys.*, 2005, **311**, 187–201.
37 N. Gaston, P. Schwerdtfeger, T. Saue and J. Greif, *J. Chem. Phys.*, 2006, **124**, 044304.
38 J. Henriksson, T. Saue and P. Norman, *J. Chem. Phys.*, 2008, **128**, 024105.
39 R. Bast, A. J. Thorvaldsen, M. Ringholm and K. Ruud, *Chem. Phys.*, 2009, **356**, 177–186.
40 R. Bast, U. Ekstrom, B. Gao, T. Helgaker, K. Ruud and A. J. Thorvaldsen, *Phys. Chem. Chem. Phys.*, 2011, **13**, 2627–2651.
41 J. Gao, W. Liu, B. Song and C. Liu, *J. Chem. Phys.*, 2004, **121**, 6658–6666.
42 J. Gao, W. Zou, W. Liu, Y. Xiao, D. Peng, B. Song and C. Liu, *J. Chem. Phys.*, 2005, **123**, 054102.
43 R. Bast, H. J. Aa. Jensen and T. Saue, *Int. J. Quantum Chem.*, 2009, **109**, 2091–2112.
44 M. Repisky, S. Komorovsky, E. Malkin, O. L. Malkina and V. G. Malkin, *Chem. Phys. Lett.*, 2010, **488**, 94–97.
45 S. Komorovsky, M. Repisky, O. L. Malkina and V. G. Malkin, *J. Chem. Phys.*, 2010, **132**, 154101.
46 L. Cheng, Y. Xiao and W. Liu, *J. Chem. Phys.*, 2009, **131**, 244113.
47 M. Iliaš and T. Saue, *J. Chem. Phys.*, 2007, **126**, 064102.
48 B. A. Hess, *Phys. Rev. A: At., Mol., Opt. Phys.*, 1985, **32**, 756–763.
49 B. A. Hess, *Phys. Rev. A: At., Mol., Opt. Phys.*, 1986, **33**, 3742–3748.
50 E. van Lenthe, E. J. Baerends and J. G. Snijders, *J. Chem. Phys.*, 1993, **99**, 4597–4610.
51 E. van Lenthe, E. J. Baerends and J. G. Snijders, *J. Chem. Phys.*, 1994, **101**, 9783–9792.
52 E. van Lenthe, J. G. Snijders and E. J. Baerends, *J. Chem. Phys.*, 1996, **105**, 6505–6516.
53 ADF2010, SCM,Theoretical Chemistry, Vrije Universiteit, Amsterdam, The Netherlands, http://www.scm.com.
54 T. Belling, T. Grauschopf, S. Kroeger, F. Nörtemann, M. Staufer, M. Mayer, V. A. Nasluzov, U. Birkenheuer, A. Hu, A. Matveev, A.V. Shor, M. Fuchs-Rohr, K. M. Neyman, D. I. Ganyushin, T. Kerdcharoen, A. Woiterski, S. Majumder and N. Roesch, Paragauss, ParaGauss was developed at Technical University of Munich.
55 W. Liu, *Mol. Phys.*, 2010, **108**, 1679.
56 W. Liu and D. Peng, *J. Chem. Phys.*, 2006, **125**, 044102.
57 D. Peng, W. Liu, T. Xiao and L. Cheng, *J. Chem. Phys.*, 2007, **127**, 104106.
58 M. Iliaš, V. Kellö and M. Urban, *Acta Phys. Slovaca*, 2010, **60**, 259–391.
59 T. Saue, K. Fegri, T. Helgaker and O. Gropen, *Mol. Phys.*, 1997, **91**, 937.
60 T. Nakajima and K. Hirao, *J. Chem. Phys.*, 2004, **121**, 3438–3445.
61 S. Varga, E. Engel, W. Sepp and B. Fricke, *Phys. Rev. A: At., Mol., Opt. Phys.*, 1999, **59**, 4288–4294.
62 L. Visscher, *Theor. Chem. Acc.*, 1997, **98**, 68.
63 W. Liu, F. Wang and L. Li, *J. Theor. Comput. Chem.*, 2003, **2**, 257–272.
64 L. Belpassi, F. Tarantelli, A. Sgamellotti and H. M. Quiney, *J. Chem. Phys.*, 2006, **124**, 124104.
65 J. W. Mintmire and B. I. Dunlap, *Phys. Rev. A: At., Mol., Opt. Phys.*, 1982, **25**, 88–95.
66 F. R. Manby and P. J. Knowles, *Phys. Rev. Lett.*, 2001, **87**, 163001.
67 L. Belpassi, F. Tarantelli, A. Sgamellotti and H. M. Quiney, *J. Chem. Phys.*, 2008, **128**, 124108.
68 L. Belpassi, F. Tarantelli, A. Sgamellotti and H. M. Quiney, *Phys. Rev. B: Condens. Matter*, 2008, **77**, 233403.
69 L. Storchi, L. Belpassi, F. Tarantelli, A. Sgamellotti and H. M. Quiney, *J. Chem. Theory Comput.*, 2010, **6**, 384–394.
70 M. Mayer, O. D. Häberlen and N. Rösch, *Phys. Rev. A: At., Mol., Opt. Phys.*, 1996, **54**, 4775–4782.
71 A. Rosén and D. E. Ellis, *Chem. Phys. Lett.*, 1974, **27**, 595–599.
72 A. Rosén and D. E. Ellis, *J. Chem. Phys.*, 1975, **62**, 3039–3049.
73 C. Y. Yang and S. Rabii, *Phys. Rev. A: At., Mol., Opt. Phys.*, 1975, **12**, 362–369.
74 D. A. Case and C. Y. Yang, *J. Chem. Phys.*, 1980, **72**, 3443–3448.
75 B. G. Cartling and D. M. Whitmore, *Chem. Phys. Lett.*, 1975, **35**, 51–56.
76 B. G. Cartling and D. M. Whitmore, *Int. J. Quantum Chem.*, 1976, **10**, 393–412.
77 R. Arratia-Perez and D. A. Case, *Inorg. Chem.*, 1984, **23**, 3271–3273.
78 A. F. Ramos, R. Arratia-Perez and G. L. Malli, *Phys. Rev. B: Condens. Matter*, 1987, **35**, 3790–3798.
79 R. Arratia-Pérez and L. Hernández-Acevedo, *Chem. Phys. Lett.*, 1999, **303**, 641–648.
80 A. Rosén, B. Fricke and T. Morović, *Phys. Rev. Lett.*, 1978, **40**, 856–859.
81 W.-D. Sepp and B. Fricke, *Phys. Scr.*, 1987, **36**, 268.
82 T. Bastugt, W. D. Sepp, D. Kolb, B. Fricke, E. J. Baerends and G. T. Velde, *J. Phys. B: At., Mol. Opt. Phys.*, 1995, **28**, 2325.
83 T. Bastugt, K. Rashid, W.-D. Sepp, D. Kolb and B. Fricke, *Phys. Rev. A: At., Mol., Opt. Phys.*, 1997, **55**, 1760–1764.
84 S. Varga, E. Engel, W.-D. Sepp and B. Fricke, *Phys. Rev. A: At., Mol., Opt. Phys.*, 1999, **59**, 4288–4294.
85 W. Liu and C. van Wüllen, *J. Chem. Phys.*, 2000, **113**, 2506–2507.
86 S. Varga, B. Fricke, H. Nakamatsu, T. Mukoyama, J. Anton, D. Geschke, A. Heitmann, E. Engel and T. Bastug, *J. Chem. Phys.*, 2000, **112**, 3499–3506.
87 S. Varga, A. Rosén, W.-D. Sepp and B. Fricke, *Phys. Rev. A: At., Mol., Opt. Phys.*, 2001, **63**, 022510.
88 D. Geschke, T. Baştuğ, T. Jacob, S. Fritzsche, W.-D. Sepp, B. Fricke, S. Varga and J. Anton, *Phys. Rev. B: Condens. Matter*, 2001, **64**, 235411.
89 J. Anton, B. Fricke and P. Schwerdtfeger, *Chem. Phys.*, 2005, **311**, 97–103.

90 J. Anton, B. Fricke and E. Engel, *Phys. Rev. A: At., Mol., Opt. Phys.*, 2004, **69**, 012505.
91 J. Anton, T. Ishii and B. Fricke, *Chem. Phys. Lett.*, 2004, **388**, 248–252.
92 J. Anton, T. Jacob, B. Fricke and E. Engel, *Phys. Rev. Lett.*, 2002, **89**, 213001.
93 V. Pershina, A. Borschevsky, J. Anton and T. Jacob, *J. Chem. Phys.*, 2010, **133**, 104304.
94 V. Pershina, J. Anton and T. Jacob, *J. Chem. Phys.*, 2009, **131**, 084713.
95 V. Pershina, J. Anton and B. Fricke, *J. Chem. Phys.*, 2007, **127**, 134310.
96 V. Pershina, J. Anton and T. Bastug, *Eur. Phys. J. D*, 2007, **45**, 87–90.
97 V. Pershina, J. Anton and T. Jacob, *Phys. Rev. A: At., Mol., Opt. Phys.*, 2008, **78**, 032518.
98 F. Wang and W. Liu, *J. Chin. Chem. Soc. (Taipei)*, 2003, **50**(3B), 597.
99 D. Peng, J. Ma and W. Liu, *Int. J. Quantum Chem.*, 2009, **109**, 2149–2167.
100 T. Yanai, T. Nakajima, Y. Ishikawa and K. Hirao, *J. Chem. Phys.*, 2002, **116**, 10122–10128.
101 T. Nakajima and K. Hirao, *Monatsh. Chem.*, 2005, **136**, 965–986.
102 T. Yanai, H. Nakano, T. Nakajima, T. Tsuneda, S. Hirata, Y. Kawashima, Y. Nakao, M. Kamiya, H. Sekino and K. Hirao, *Lect. Notes Comput. Sci.*, 2003, **2660**, 84–95.
103 T. Yanai, K. Ishida, H. Nakano and K. Hirao, *Int. J. Quantum Chem.*, 2000, **76**, 396.
104 K. Ishida, *J. Chem. Phys.*, 1999, **111**, 4913.
105 M. Head-Gordon and J. A. Pople, *J. Chem. Phys.*, 1988, **89**, 5777–5786.
106 T. Tsuneda and K. Hirao, *Chem. Phys. Lett.*, 1997, **268**, 510.
107 R. A. Friesner, *J. Chem. Phys.*, 1986, **85**, 1462–1468.
108 T. Yanai, R. J. Harrison, T. Nakajima, Y. Ishikawa and K. Hira, *Int. J. Quantum Chem.*, 2007, **107**, 1382–1389.
109 DIRAC, a relativistic *ab initio* electronic structure program, Release DIRAC10 (2010), written by T. Saue, L. Visscher and H. J. Aa. Jensen, with contributions from R. Bast, K. G. Dyall, U. Ekström, E. Eliav, T. Enevoldsen, T. Fleig, A. S. P. Gomes, J. Henriksson, M. Iliaš, Ch. R. Jacob, S. Knecht, H. S. Nataraj, P. Norman, J. Olsen, M. Pernpointner, K. Ruud, B. Schimmelpfennig, J. Sikkema, A. Thorvaldsen, J. Thyssen, S. Villaume and S. Yamamoto (see http://dirac.chem.vu.nl).
110 T. Saue and H. J. A. Jensen, *J. Chem. Phys.*, 1999, **111**, 6211–6222.
111 T. Helgaker, P. R. Taylor and K. Ruud, *HERMIT: A molecular integral program*, 1995.
112 A. D. Becke, *J. Chem. Phys.*, 1988, **88**, 2547–2553.
113 M. Grüning, O. V. Gritsenko, S. J. A. van Gisbergen and E. J. Baerends, *J. Chem. Phys.*, 2001, **114**, 652–660.
114 P. R. T. Schipper, O. V. Gritsenko, S. J. A. van Gisbergen and E. J. Baerends, *J. Chem. Phys.*, 2000, **112**, 1344–1352.
115 O. Fossgaard, O. Gropen, M. Valero and T. Saue, *J. Chem. Phys.*, 2003, **118**, 10418–10430.
116 R. Bast, A. Koers, A. S. P. Gomes, M. Ilias, L. Visscher, P. Schwerdtfeger and T. Saue, *Phys. Chem. Chem. Phys.*, 2011, **13**, 864–876.
117 D. Figgen, T. Saue and P. Schwerdtfeger, *J. Chem. Phys.*, 2010, **132**, 234310.
118 S. Villaume, T. Saue and P. Norman, *J. Chem. Phys.*, 2010, **133**, 064105.
119 E. Runge and E. K. U. Gross, *Phys. Rev. Lett.*, 1984, **52**, 997.
120 U. Ekstrom, L. Visscher, R. Bast, A. J. Thorvaldsen and K. Ruud, *J. Chem. Theory Comput.*, 2010, **6**, 1971–1980.
121 R. Bast, J. Juselius and T. Saue, *Chem. Phys.*, 2009, **356**, 187–194.
122 R. Bast, *Quantum Chemistry Beyond the Charge Density*, *PhD thesis*, Universitè Louis Pasteur, Strasbourg, 2008.
123 M. Repisky, S. Komorovsky, O. L. Malkina and V. G. Malkin, *Chem. Phys.*, 2009, **356**, 236–242.
124 S. Suzuki and K. Nakao, *J. Phys. Soc. Jpn.*, 1999, **68**, 1982–1987.
125 S. Suzuki and H. Ohta, *J. Phys. Soc. Jpn.*, 2010, **79**, 074703.
126 T. Huhne, C. Zecha, H. Ebert, P. H. Dederichs and R. Zeller, *Phys. Rev. B: Condens. Matter*, 1998, **58**, 10236–10247.
127 A. Dal Corso, *Phys. Rev. B: Condens. Matter*, 2010, **82**, 075116.
128 H. Schring, M. Richter and I. Opahle, in *Relativistic Electronic Structure Theory, Part II: Applications Recent Development and Applications in Density Functional Theory*, ed. P. Schwerdtfeger, Elsevier, 2004, vol. 2, pp. 723–776.
129 N. Gaston, I. Opahle, H. Gäggeler and P. Schwerdtfeger, *Angew. Chem., Int. Ed.*, 2007, **46**, 1663–1666.
130 L. E. McMurchie and E. R. Davidson, *J. Comput. Phys.*, 1978, **26**, 218–231.
131 V. R. Saunders, in *Methods in Computational Molecular Physics*, ed. G. H. F. Diercksen and S. Wilson, Reidel Publishing Company, Dordrecht, 1983, p. 1.
132 K. G. Dyall and K. J. Faegri, *Chem. Phys. Lett.*, 1990, **174**, 25.
133 E. U. Condon and G. H. Shortley, *The Theory of Atomic Spectra*, Cambridge University Press, Cambridge, 1951.
134 L. Visscher and K. G. Dyall, *At. Data Nucl. Data Tables*, 1997, **67**, 207.
135 I. P. Grant and H. M. Quiney, *Adv. At. Mol. Phys.*, 1988, **23**, 37.
136 H. M. Quiney, H. Skaane and I. P. Grant, *Adv. Quantum Chem.*, 1999, **32**, 1.
137 I. P. Grant and H. M. Quiney, *Int. J. Quantum Chem.*, 2000, **80**, 283.
138 H. M. Quiney and I. P. Grant, to be published.
139 V. I. Lebedev and D. N. Laikov, *Dokl. Math.*, 1999, **59**, 477.
140 J. Almlöf, *J. Chem. Phys.*, 1996, **104**, 4685.
141 G. R. Ahmadi and J. Almlöf, *Chem. Phys. Lett.*, 1996, **246**, 364.
142 K. Eichkorn, O. Treutler, H. Öhm, M. Häser and R. Ahlrichs, *Chem. Phys. Lett.*, 1995, **240**, 283.
143 B. I. Dunlap, J. W. D. Connoly and J. R. Sabin, *J. Chem. Phys.*, 1979, **71**, 4993.
144 J. W. Mintmire and B. I. Dunlap, *Phys. Rev. A: At., Mol., Opt. Phys.*, 1982, **25**, 88.
145 A. St-Amant and D. R. Salahub, *Chem. Phys. Lett.*, 1990, **169**, 387.
146 O. Vahtras, J. Almlöf and M. W. Feyereisen, *Chem. Phys. Lett.*, 1993, **213**, 514.
147 F. R. Manby and P. J. Knowles, *Phys. Rev. Lett.*, 2001, **87**, 163001.
148 *deMon2k version 2006*, a package for Density Functional Theory.
149 A. Köster, J. U. Reveles and J. M. del Campo, *J. Chem. Phys.*, 2004, **121**, 3417.
150 B. I. Dunlap, J. Andzelm and J. W. Mintmire, *Phys. Rev. A: At., Mol., Opt. Phys.*, 1990, **42**, 6354.
151 D. N. Laikov, *Chem. Phys. Lett.*, 1997, **281**, 151.
152 U. Birkenheuer, A. B. Gordienko, V. A. Nasluzov, M. K. Fuchs-Rohr and N. Rösch, *Int. J. Quantum Chem.*, 2005, **102**, 743.
153 Silicon Graphics, *Powering the Real-time Enterprise*, Silicon Graphics White Paper 3935, 2006.
154 Message Passing Interface Forum. University of Tennessee, *MPI: A Message-Passing Interface Standard. Version 2.2*, 2009.
155 L. S. Blackford, J. Choi, A. Cleary, E. D'Azevedo, J. Demmel, I. Dhillon, J. Dongarra, S. Hammarling, G. Henry, A. Petitet, K. Stanley, D. Walker and R. C. Whaley, *ScaLAPACK Users' Guide*, Society for Industrial and Applied Mathematics, Philadelphia, PA, 1997.
156 M. Schädel, *Angew. Chem., Int. Ed.*, 2006, **45**, 368–401.
157 K. G. Dyall, *Theor. Chem. Acc.*, 2004, **112**, 403–409.
158 K. G. Dyall, personal communication.
159 A. Becke, *Phys. Rev. A: At., Mol., Opt. Phys.*, 1988, **38**, 3098.
160 C. Lee, W. Yang and R. G. Parr, *Phys. Rev. B: Condens. Matter*, 1988, **37**, 785.
161 F. Tarantelli, L. Belpassi and L. Storchi, *Parallel Computing: From Multicores and GPU's to Petascale*, Amsterdam, 2010, pp. 501–512.
162 L. Storchi, L. Belpassi and F. Tarantelli, to be published.
163 J. Choi, J. Demmel, I. Dhillon, J. Dongarra, S. Ostrouchov, A. Petitet, K. Stanley, D. Walker and R. C. Whaley, *Comput. Phys. Commun.*, 1996, **97**, 1–15.
164 I. S. Ufimtsev and T. J. Martinez, *J. Chem. Theory Comput.*, 2009, **5**, 1004–1015.
165 http://www.nvidia.com/content/cudazone/cuda_sdk/Linear_Algebra.html.
166 http://www.culatools.com/.
167 C. H. Keitel, *Contemp. Phys.*, 2001, **42**, 353–363.
168 A. Maquet and R. Grobe, *J. Mod. Opt.*, 2002, **49**, 2001.

169 C. J. Joachain, N. J. Kylstra and R. M. Potvliege, *J. Mod. Opt.*, 2003, **50**, 313–329.
170 Y. I. Salamin, S. X. Hu, K. Z. Hatsagortsyan and C. H. Keitel, *Phys. Rep.*, 2006, **427**, 41–155.
171 S. X. Hu and C. H. Keitel, *Phys. Rev. A: At., Mol., Opt. Phys.*, 2001, **63**, 053402.
172 S. Selstø, E. Lindroth and J. Bengtsson, *Phys. Rev. A: At., Mol., Opt. Phys.*, 2009, **79**, 043418.
173 P. W. Atkins and R. S. Friedman, *Molecular Quantum Mechanics*, Oxford University Press, New York, 1997.
174 S. Salomonson and P. Öster, *Phys. Rev. A: At., Mol., Opt. Phys.*, 1989, **40**, 5548–5558.
175 R. Stacey, *Phys. Rev. D: Part. Fields*, 1982, **26**, 468–472.
176 W. R. Johnson, S. A. Blundell and J. Sapirstein, *Phys. Rev. A: At., Mol., Opt. Phys.*, 1988, **37**, 307–315.
177 J. J. Sakurai, *Advanced Quantum Mechanics*, Addison-Wiley, London, 1967.
178 W. Kutzelnigg, *Phys. Rev. A: At., Mol., Opt. Phys.*, 2003, **67**, 032109.
179 G. A. Aucar, T. Saue, L. Visscher and H. J. A. Jensen, *J. Chem. Phys.*, 1999, **110**, 6208–6218.
180 A. Castro, M. Marques and A. Rubio, *J. Chem. Phys.*, 2004, **121**, 3425–3433.
181 W. H. Press, S. A. Teukolsky, W. T. Vetterling and B. P. Flannery, *Numerical Recipes in Fortran: The art of scientific computing*, Cambridge University Press, Cambridge CB2 1RP, United Kingdom, 1992.
182 J. D. Jackson, *Classical Electrodynamics (Third Edition)*, John Wiley and Sons, Inc, New York, NY, 1999.
183 G. R. Mocken and C. H. Keitel, *Comput. Phys. Commun.*, 2005, **166**, 171–190.
184 E. Runge and E. K. U. Gross, *Phys. Rev. Lett.*, 1984, **52**, 997.
185 A. Rubio and M. Marques, *Phys. Chem. Chem. Phys.*, 2009, **11**, 4481.
186 M. Casida, in *Recent Development and Applications in Density-Functional Theory*, ed. J. M. Seminario, Elsevier, 1996, vol. 1, p. 1.
187 S. Hirata and M. Head-Gordon, *Chem. Phys. Lett.*, 1999, **314**, 291–299.
188 J. Sun, J. Song, Y. Zhao and W.-Z. Liang, *J. Chem. Phys.*, 2007, **127**, 234107.
189 C.-L. Cheng, J. S. Evans and T. Van Voorhis, *Phys. Rev. B: Condens. Matter*, 2006, **74**, 155112.
190 M. A. L. Marques, A. Castro, G. F. Bertsch and A. Rubio, *Comput. Phys. Commun.*, 2003, **151**, 60–78.
191 K. Yabana and G. F. Bertsch, *Phys. Rev. B: Condens. Matter*, 1996, **54**, 4484–4487.
192 K. Yabana, T. Nakatsukasa, J. Iwata and G. Bertsch, *Phys. Status Solidi B*, 2006, **243**, 1121–1138.
193 C. M. Isborn and X. Li, *J. Chem. Theory Comput.*, 2009, **5**, 2415–2419.
194 A. Tsolakidis, D. Sanchez-Portal and R. Martin, *Phys. Rev. B: Condens. Matter*, 2002, **66**, 235416.
195 Y. Takimoto, F. D. Vila and J. J. Rehr, *J. Chem. Phys.*, 2007, **127**, 154114.
196 T. Akama, Y. Imamura and H. Nakai, *Chem. Lett.*, 2010, 407–409.
197 J. Sun, J. Liu, W. Liang and Y. Zhao, *J. Phys. Chem. A*, 2008, **112**, 10442–10447.
198 J. Liu, Z. Guo, J. Sun and W. Liang, *Front. Chem. China*, 2010, **5**, 11–28.
199 K. Nobusada and K. Yabana, *Phys. Rev. A: At., Mol., Opt. Phys.*, 2007, **75**, 032518.
200 M. Casida, in *Recent Advances in Density Functional Methods*, ed. D. P. ChongWorld Scientific, Singapore, 1995, vol. 1, pp. 155–192.
201 A. D. Bandrauk, S. Chelkowski, D. J. Diestler, J. Manz and K.-J. Yuan, *Phys. Rev. A: At., Mol., Opt. Phys.*, 2009, **79**, 023403.
202 R. G. Parr and W. Yang, *Density-functional Theory of Atoms and Molecules*, Oxford University Press, Oxford, 1989.
203 H. Eschring and V. D. P. Servedio, *J. Comput. Chem.*, 1999, **20**, 23–30.
204 C. van Wüllen, *J. Comput. Chem.*, 2002, **23**, 779–785.
205 R. Bast, T. Saue, J. Henriksson and P. Norman, *J. Chem. Phys.*, 2009, **130**, 024109.
206 E. Engel, S. Keller and R. M. Dreizler, *Phys. Rev. A: At., Mol., Opt. Phys.*, 1996, **53**, 1367–1374.
207 O. Fossgaard, O. Gropen, E. Eliav and T. Saue, *J. Chem. Phys.*, 2003, **119**, 9355–9363.
208 L. Belpassi, F. Tarantelli, A. Sgamellotti and H. M. Quiney, *J. Phys. Chem. A*, 2006, **110**, 4543–4554.
209 C. Thierfelder, P. Schwerdtfeger, A. Koers, A. Borschevsky and B. Fricke, *Phys. Rev. A: At., Mol., Opt. Phys.*, 2009, **80**, 022501.
210 P. Schwerdtfeger, R. Bast, M. C. L. Gerry, C. R. Jacob, M. Jansen, V. Kellö, A. V. Mudring, A. J. Sadlej, T. Saue, T. Söhnel and F. E. Wagner, *J. Chem. Phys.*, 2005, **122**, 124317.
211 P. Schwerdtfeger, M. Pernpointner and J. K. Laerdahl, *J. Chem. Phys.*, 1999, **111**, 3357–3364.
212 L. Belpassi, F. Tarantelli, A. Sgamellotti, A. W. Götz and L. Visscher, *Chem. Phys. Lett.*, 2007, **442**, 233–237.
213 E. Goll, H. Stoll, C. Thierfelder and P. Schwerdtfeger, *Phys. Rev. A: At., Mol., Opt. Phys.*, 2007, **76**, 032507.
214 A. Görling, *J. Chem. Phys.*, 2005, **123**, 062203.
215 J. D. Talman and W. F. Shadwick, *Phys. Rev. A: At., Mol., Opt. Phys.*, 1976, **14**, 36–40.
216 E. Engel, A. F. Bonetti, S. Keller, I. Andrejkovics and R. M. Dreizler, *Phys. Rev. A: At., Mol., Opt. Phys.*, 1998, **58**, 964–992.
217 J. B. Krieger, Y. Li and G. J. Iafrate, *Phys. Lett. A*, 1990, **146**, 256–260.
218 D. Ködderitzsch, H. Ebert and E. Engel, *Phys. Rev. B: Condens. Matter*, 2008, **77**, 045101.
219 E. Engel, D. Ködderitzsch and H. Ebert, *Phys. Rev. B: Condens. Matter*, 2008, **78**, 235123.
220 F. D. Sala and A. Görling, *J. Chem. Phys.*, 2001, **115**, 5718–5732.
221 A. Hesselmann and F. R. Manby, *J. Chem. Phys.*, 2005, **123**, 164116.
222 G. Vignale and M. Rasolt, *Phys. Rev. Lett.*, 1987, **59**, 2360–2363.
223 G. Vignale and M. Rasolt, *Phys. Rev. B: Condens. Matter*, 1988, **37**, 10685–10696.
224 K. Bencheikh, *J. Phys. A: Math. Gen.*, 2003, **36**, 11929–11936.
225 S. H. Abedinpour, G. Vignale and I. V. Tokatly, *Phys. Rev. B: Condens. Matter*, 2010, **81**, 125123.
226 H. Eschrig, G. Seifert and P. Ziesche, *Solid State Commun.*, 1985, **56**, 777–780.

